Global Health Care
WISDOM ACADEMIC https://doi.org/10.63808/ghc.v2i1.524 Volume 2 , Issue 1

Research Article

Mitochondrial DNA Sensing Reshapes the Tumor Immune Microenvironment via Cooperative cGAS-STING Activation and Ferroptosis

Gang Liu[1,*], Jia Wang[2], Liqiang An[3]
[1]International Sakharov Environmental Institute, Belarus State University, Minsk 220114, Belarus
[2]School of Taishan Vocational and Technical College, Tai'an 271000, China
[3]Volga State Pedagogical University, Volgograd 400005, Russia
[*]**Correspondence:** Gang Liu, lg6666699@163.com

Abstract

Abnormal release of mitochondrial DNA (mtDNA) and innate immune sensing play key roles in tumor immune regulation, but how they work together with ferroptosis is still unclear. This study aims to clarify the molecular mechanism of how mtDNA reshapes the tumor immune microenvironment in coordination with ferroptosis through activating the cGAS-STING signaling pathway, as well as its anti-tumor potential. By creating tumor cell mitochondrial stress models and using CRISPR-Cas9 gene knockout, lipid peroxidation detection, single-cell transcriptome analysis, and mouse syngeneic tumor models, we systematically assessed how mtDNA release affects the cGAS-STING pathway and ferroptosis. The results showed that mitochondrial stress-induced cytoplasmic mtDNA release significantly activates the cGAS-STING pathway, upregulates type I interferons and chemokines like CXCL10, and promotes lipid peroxidation and ferroptosis by suppressing the xCT/GPX4 antioxidant axis. Ferroptotic tumor cells further release damage-associated molecules like HMGB1 and ATP, enhancing dendritic cell maturation and $CD8^+$ T cell tumor infiltration, forming a positive feedback loop of immune activation. In mouse melanoma models, combining mtDNA release with ferroptosis significantly inhibited tumor growth and extended survival, showing better results than either intervention alone. This study reveals a new mechanism where mtDNA sensing collaborates with ferroptosis via the cGAS-STING pathway to reshape the tumor immune microenvironment, providing a theoretical basis and potential targets for developing anti-tumor immunotherapies that jointly regulate innate immunity and ferroptosis.

Keywords

Mitochondrial DNA, cGAS-STING signaling pathway, Ferroptosis, Tumor immune microenvironment, Immunotherapy

1. Introduction

Tumor immunotherapy has shown significant clinical benefits in various cancers by reshaping the body's anti-tumor immune response. However, tumor cells can evade immune surveillance through multiple mechanisms, causing a considerable number of patients to be primarily or acquired resistant to existing immunotherapies. Therefore, digging into the regulatory networks of the tumor immune microenvironment (TIME) and finding key molecular events that can boost the anti-tumor immune response is one of the main tasks in current tumor immunology research.

The innate immune sensing pathway mediated by cyclic GMP-AMP synthase (cGAS) and its downstream adaptor protein, stimulator of interferon genes (STING), acts as an important bridge connecting cellular damage to adaptive immune activation. cGAS can detect abnormal double-stranded DNA appearing in the cytoplasm and then catalyze the synthesis of the second messenger 2′3′-cGAMP, which activates STING and ultimately induces the expression of type I interferons and various pro-inflammatory cytokines through the TBK1-IRF3 axis. In tumor cells, factors like genomic instability, defective DNA damage repair, and mitochondrial stress can all cause DNA to be abnormally released into the cytoplasm, thereby activating the cGAS-STING pathway. In particular, mitochondrial DNA (mtDNA), due to its circular structure and bacterial origins, is highly immunostimulatory and is considered a key mediator linking mitochondrial dysfunction to anti-tumor innate immunity. Increasing evidence suggests that cytoplasmic release of mtDNA can activate cGAS-STING signaling, promote dendritic cell maturation, and enhance $CD8^+$ T cell tumor infiltration, thereby boosting anti-tumor immune responses.

At the same time, ferroptosis, an iron-dependent form of regulated cell death characterized by lipid peroxidation, has gained a lot of attention in recent years for its role in tumor immune regulation. Unlike apoptosis, during ferroptosis, cells release a large amount of damage-associated molecular patterns (DAMPs), such as high-mobility group protein B1 (HMGB1) and ATP, which are highly immunogenic and can effectively promote antigen presentation and T cell activation. Studies have shown that inducing ferroptosis in tumor cells can not only directly kill tumor cells but also act as an immunogenic form of cell death, boosting immune activation signals in the tumor microenvironment. However, whether ferroptosis shapes the tumor immune microenvironment through innate immune sensing pathways, especially the involvement of the cGAS-STING signaling pathway, still lacks systematic research.

It's worth noting that mitochondria are not only an important source of DNA for the

cGAS-STING pathway, but also the main site where lipid peroxidation occurs during ferroptosis. Mitochondrial dysfunction can drive both mtDNA release and lipid ROS accumulation, suggesting there might be an inherent functional coupling between cGAS-STING activation and ferroptosis. However, most existing studies treat mtDNA sensing and ferroptosis as two relatively independent biological events. How they might work together to regulate anti-tumor immune responses in the tumor microenvironment, and the underlying molecular mechanisms and biological significance, are still unclear.

Based on the current research, this study proposes a scientific hypothesis: the cytoplasmic release of mtDNA induced by mitochondrial stress in tumor cells activates the cGAS-STING pathway, forming a synergistic amplification loop with ferroptosis, jointly reshaping the tumor immune microenvironment and enhancing anti-tumor immune responses. To test this hypothesis, we combined gene editing, lipid peroxidation detection, single-cell transcriptome analysis, and syngeneic tumor models to systematically explore the cross-regulation mechanism between mtDNA sensing and ferroptosis and its impact on the tumor immune microenvironment, aiming to provide new theoretical support and potential intervention targets for tumor immunotherapy strategies based on innate immunity and ferroptosis.

2. Literature Review

2.1. cGAS-STING signaling pathway and tumor immunity

The composition and dynamic changes of the tumor microenvironment (TME) have a huge impact on tumor progression and treatment response, and digging into its cellular and molecular networks is a cutting-edge area in tumor immunology research (Liu, 2026). Cyclic GMP-AMP synthase (cGAS) acts as a key sensor for cytoplasmic double-stranded DNA (dsDNA). It can catalyze the production of the second messenger 2′3′-cGAMP, which then activates the adaptor protein STING on the endoplasmic reticulum. This kicks off downstream signaling through TBK1-IRF3 and IKK-NF-κB pathways, leading to the production of type I interferons and pro-inflammatory cytokines (Ablasser et al., 2013; Chen et al., 2016). This innate immune sensing mechanism was originally discovered in antiviral immune responses, but recent studies have shown that it also plays an indispensable role in tumor immune surveillance. In the tumor microenvironment, activation of the cGAS-STING pathway can promote the maturation of dendritic cells (DCs), enhance cross-presentation of tumor antigens, and induce the secretion of chemokines like CXCL9 and CXCL10, which help recruit $CD8^+$ T cells to the tumor site, creating an ‘inflamed’ tumor microenvironment (Hopfner & Hornung, 2020; Kwon & Bakhoum, 2020). Preclinical studies show that STING agonists, either alone or combined with immune checkpoint inhibitors, can significantly inhibit the growth of various tumors, and some have already entered clinical trials (Sen et al., 2019;

Yum et al., 2021). However, the activation of the cGAS-STING pathway isn't common in tumors. Tumor cells often escape cGAS-STING detection through various mechanisms like epigenetic silencing, mutations in pathway components, or inhibitory factors in the microenvironment (Ahn et al., 2014; Zhu et al., 2014). So, figuring out how the cGAS-STING pathway gets naturally activated in tumor cells is super important for coming up with new immunotherapy strategies.

2.2. Mitochondrial DNA release and cGAS-STING activation

Mitochondria, as cell organelles with their own genome (mtDNA), are crucial for maintaining cell stability. Under conditions like oxidative stress, changes in mitochondrial membrane permeability, or inhibition of apoptosis pathways, mtDNA can be released into the cytoplasm and act as an important internal trigger for activating the cGAS-STING pathway (Riley & Tait, 2020; West et al., 2015). West and others (2017) first showed that the stress on mtDNA caused by the loss of mitochondrial transcription factor A (TFAM) can trigger a STING-dependent antiviral immune response, establishing mtDNA as a key danger signal in innate immunity. In the context of tumors, mitochondrial dysfunction in tumor cells, the accumulation of reactive oxygen species (ROS), and the opening of the mitochondrial permeability transition pore can all promote the escape of mtDNA into the cytoplasm, which in turn activates the cGAS-STING signaling pathway (Galluzzi et al., 2018; Tigano et al., 2021). Interestingly, some chemotherapy drugs (like cisplatin and paclitaxel) and radiotherapy have also been shown to activate the STING pathway by inducing mtDNA release, thereby boosting anti-tumor immune responses (Deng et al., 2014; Li et al., 2021). However, how mtDNA release works together with other stress responses in tumor cells, especially its inherent connection with immunogenic cell death, still lacks systematic research.

2.3. The role of ferroptosis in tumor immune regulation

Ferroptosis is a type of regulated cell death named by Dixon and others in 2012, which depends on iron and is characterized by the accumulation of lipid peroxides. Its morphological and biochemical features are clearly different from apoptosis, necrosis, and autophagy (Dixon et al., 2012). The core mechanism of ferroptosis involves the loss of activity of glutathione peroxidase 4 (GPX4) or the inhibition of the cystine/glutamate antiporter system Xc^- (xCT/SLC7A11), which prevents the cell from effectively clearing lipid peroxides and eventually triggers lipid membrane peroxidation and cell death (Stockwell et al., 2017; Yang et al., 2014). Ferroptosis plays a dual role in tumor development, but recent studies have shown that inducing ferroptosis in tumor cells can be an effective anti-tumor strategy, and ferroptosis is highly immunogenic. During ferroptosis, tumor cells release damage-associated molecular patterns (DAMPs) like HMGB1, ATP, and calreticulin, which can promote DC maturation and $CD8^+$ T cell activation, boosting anti-tumor immune responses (Chen et al., 2021; Jiang et al., 2021). More importantly, IFN-γ secreted by $CD8^+$ T cells can downregulate the

expression of SLC7A11 and GPX4 in tumor cells, thereby promoting ferroptosis, suggesting that ferroptosis is one of the key ways T cells kill tumor cells (Wang et al., 2019). In addition, combining radiotherapy and immunotherapy has also been shown to synergistically inhibit SLC7A11 to trigger ferroptosis, boosting anti-tumor immunity (Lang et al., 2019). However, the molecular mechanisms by which ferroptosis drives the remodeling of the tumor immune microenvironment, especially its crosstalk with innate immune sensing pathways, are still in the early stages of exploration.

2.4. The cross-regulation between cGAS-STING and ferroptosis

Although significant research progress has been made in the cGAS-STING signaling pathway and ferroptosis individually, the functional connection between the two has only started to gain attention in recent years. On one hand, STING activation may promote ferroptosis by inducing lipid peroxidation or regulating iron metabolism. Studies have found that STING agonists can upregulate ACSL4 expression and promote the oxidation of polyunsaturated fatty acids, thereby enhancing sensitivity to ferroptosis (Jia et al., 2020). On the other hand, mitochondrial damage and mtDNA release during ferroptosis can, in turn, activate the cGAS-STING pathway, creating a positive feedback loop. A recent study by Li and colleagues (2025) demonstrated for the first time that mitochondrial DNA stress can trigger autophagic ferroptosis in a STING1-dependent manner, suggesting a direct molecular link between mtDNA sensing and ferroptosis. In addition, GPX4, as a key inhibitor of ferroptosis, has also been found to promote STING activation by maintaining redox balance, further suggesting a deep intertwining of the two pathways at the redox level. However, most of these studies were done in vitro or in non-tumor models, and the collaboration between mtDNA sensing and ferroptosis in the tumor immune microenvironment, as well as its impact on anti-tumor immune responses, hasn't been systematically explored yet.

2.5. Limitations of existing research and this study's contributions

In summary, existing research has established the important roles of the cGAS-STING pathway and ferroptosis in tumor immune regulation, and has preliminarily revealed a possible cross-regulatory relationship between the two. However, the following key questions remain unanswered: Is there a functional synergy between mtDNA release activating the cGAS-STING pathway and ferroptosis in tumor cells, and what is the molecular mechanism? Can this synergy reshape the tumor immune microenvironment, especially affecting DC maturation and $CD8^+$ T cell infiltration? Could targeting this synergistic axis have anti-tumor potential in vivo, and could it offer a new strategy to overcome immunotherapy resistance?

To address the shortcomings mentioned above, this study builds a mitochondrial stress model in tumor cells and combines it with explainable spatial AI to analyze tumor-immune interactions using emerging technical concepts (Liu et al., 2026). This study systematically explores the cross-regulation

mechanism between mtDNA sensing and ferroptosis, as well as its immunological consequences. The innovative contributions of this research are reflected in three aspects: for the first time, it clarifies the molecular pathway by which mtDNA activates the cGAS-STING pathway to promote ferroptosis, revealing a positive feedback amplification loop between the two pathways in tumor cells; from the perspective of the immune microenvironment, it shows that this synergy can enhance tumor immunogenicity, promoting DC maturation and $CD8^+$ T cell infiltration, thus linking innate immune sensing with adaptive immune responses; at the in vivo level, it validates that targeting the mtDNA-cGAS-STING-ferroptosis axis can significantly inhibit tumor growth, providing a theoretical basis and potential intervention targets for developing new immunotherapy strategies based on the combined regulation of innate immunity and ferroptosis.

3. Materials and Methods

3.1. Cell lines and culture conditions

The mouse melanoma cell line B16-F10, mouse colon cancer cell line MC38, and human embryonic kidney epithelial cell line HEK293T were all purchased from the American Type Culture Collection (ATCC). B16-F10 and MC38 cells were cultured in high-glucose DMEM supplemented with 10% fetal bovine serum (FBS, Gibco), 100 U/mL penicillin, and 100 μg/mL streptomycin, and kept in a 37 °C incubator with 5% CO_2. HEK293T cells were cultured in DMEM with 10% FBS. All cells were regularly tested for mycoplasma to confirm they were contamination-free.

3.2. Main reagents and antibodies

DMEM high-glucose medium, fetal bovine serum (FBS), and phosphate-buffered saline (PBS) were purchased from Gibco. Cell lysis buffer RIPA, protease inhibitor cocktail, and phosphatase inhibitors were purchased from Thermo Fisher Scientific. Polybrene and puromycin were purchased from Sigma-Aldrich. Mitochondrial stress inducers oligomycin, antimycin A, and the mitochondrial uncoupler CCCP were purchased from MedChemExpress. Ferroptosis inducers erastin and RSL3 were purchased from Selleck Chemicals. Ferroptosis inhibitors ferrostatin-1 (Fer-1) and deferoxamine (DFO) were purchased from Sigma-Aldrich. The STING agonist cGAMP was purchased from InvivoGen. The STING inhibitor H-151 was purchased from MedChemExpress. The lipid peroxidation probe C11-BODIPY (581/591) was purchased from Thermo Fisher Scientific. Malondialdehyde (MDA) assay kits and glutathione (GSH/GSSG) assay kits were purchased from Nanjing Jiancheng Bioengineering Institute. Iron content assay kits (FerroZine method) were purchased from Abcam.

Antibody information: Rabbit anti-cGAS monoclonal antibody (#31659, Cell Signaling Technology), rabbit anti-STING monoclonal antibody (#13647, CST), rabbit anti-phospho-STING

(Ser365) antibody (#72971, CST), rabbit anti-TBK1 antibody (#3504, CST), rabbit anti-phospho-TBK1 (Ser172) antibody (#5483, CST), rabbit anti-IRF3 antibody (#4302, CST), rabbit anti-phospho-IRF3 (Ser396) antibody (#29047, CST), rabbit anti-GPX4 antibody (#52455, CST), rabbit anti-xCT/SLC7A11 antibody (#12691, CST), rabbit anti-ACSL4 antibody (#22401, CST), rabbit anti-TFAM antibody (#8076, CST), mouse anti-β-actin antibody (#3700, CST). Flow cytometry antibodies: anti-CD45-PerCP-Cy5.5 (clone 30-F11), anti-CD3-FITC (clone 17A2), anti-CD8a-APC (clone 53-6.7), anti-CD4-PE (clone GK1.5), anti-CD11c-PE-Cy7 (clone N418), anti-MHC-II (I-A/I-E)-APC-eFluor780 (clone M5/114.15.2), anti-CD86-BV421 (clone GL-1), anti-IFN-γ-BV650 (clone XMG1.2), anti-TNF-α-BV605 (clone MP6-XT22), all purchased from BioLegend. Cytokine ELISA kits (mouse IFN-β, CXCL10/IP-10, IL-6, TNF-α) were purchased from R&D Systems.

3.3. Experimental animals

Female C57BL/6J mice aged 6-8 weeks were purchased from Beijing Vital River Laboratory Animal Technology Co., Ltd. They were kept in a specific pathogen-free (SPF) animal facility under constant temperature (22±2°C) and humidity (55%±5%) with a 12-hour light-dark cycle, and had free access to food and water.

3.4. Detection of mitochondrial stress induction and mtDNA release

To trigger mitochondrial stress in tumor cells and the release of mtDNA into the cytoplasm, the following three methods were used: treating cells with oligomycin (10 μM) combined with antimycin A (10 μM) for 6 hours to inhibit mitochondrial oxidative phosphorylation; treating cells with CCCP (20 μM) for 4 hours to disrupt mitochondrial membrane potential; knocking down mitochondrial transcription factor A (TFAM) using CRISPR-Cas9 to induce mtDNA replication stress. After treatment, cytoplasmic fractions were separated using a mitochondrial isolation kit (Thermo Fisher), cytoplasmic DNA was extracted using the QIAamp DNA Mini Kit (Qiagen), and mtDNA copy number was measured by real-time quantitative PCR (primer sequences: mouse mt-Co1 forward 5′-GCCCCAGATATAGCATTCCC-3′, reverse 5′-GTTCATCCTGTTCCTGCTCC-3′; mouse nuclear gene Tert as internal control). Relative mtDNA abundance was calculated using the ΔCt method.

3.5. CRISPR-Cas9 gene knockout and lentiviral transduction

Design single-guide RNAs (sgRNAs) for mouse cGAS (gene name Mb21d1), STING (gene name Tmem173), TFAM, and SLC7A11, and clone them into the lentiCRISPR v2 vector (Addgene #52961). The sgRNA target sequences are as follows: cGAS sgRNA: 5′-GACCGAGCTCACCGCCAAGA-3′; STING sgRNA: 5′-GCTGCTCGCCAGCTACTATC-3′; TFAM sgRNA: 5′-GCTCCCCCTTCAGTTTTGTG-3′; SLC7A11 sgRNA: 5′-GATGCTGTACTATTTGGGCC-3′. Co-transfect the recombinant plasmids with the packaging

plasmids psPAX2 (Addgene #12260) and pMD2.G (Addgene #12259) into HEK293T cells, collect viral supernatant at 48 and 72 hours, filter through a 0.45 μm filter, and then use it to infect target cells with 8 μg/mL polybrene. After 48 hours of infection, select stable knockout cell lines using puromycin (2 μg/mL), and check knockout efficiency by Western blot. Control cells were transduced with the lentiCRISPR v2 vector carrying a non-targeting sgRNA (5′-GCGAGGTATTCGGCTCCGCG-3′).

3.6. Cell viability and cell death detection

Cell viability was measured using the CCK-8 kit (Dojindo). Tumor cells were seeded at 5×10^3 per well in a 96-well plate, allowed to adhere overnight, and then given the appropriate treatments. At specified time points, 10 μL of CCK-8 solution was added, incubated at 37 °C for 2 hours, and the absorbance at 450 nm was measured using a microplate reader (BioTek Synergy H1). Cell death was detected using the lactate dehydrogenase (LDH) release method (CytoTox 96 Non-Radioactive Cytotoxicity Assay, Promega) following the manufacturer's instructions. Apoptosis and necrosis were analyzed by flow cytometry using the Annexin V-FITC/PI double staining kit (BD Biosciences). The proportion of ferroptotic cells was indicated by the oxidation signal of the C11-BODIPY probe.

3.7. Lipid peroxidation detection

The level of lipid peroxidation in cells was measured using the C11-BODIPY (581/591) probe. Cells were seeded at 2×10^5 per well in a 6-well plate. After treatment, they were washed with PBS and incubated with 2 μM C11-BODIPY at 37 °C in the dark for 30 minutes. Cells were then collected after digestion, washed twice with PBS, and analyzed using a flow cytometer (BD FACSVerse) to detect fluorescence in the FITC channel (oxidized C11-BODIPY, excitation/emission 488/510 nm), with the mean fluorescence intensity (MFI) representing the level of lipid peroxidation. Malondialdehyde (MDA) content was measured using the thiobarbituric acid (TBA) method. Lysates from 1×10^6 cells were processed according to the kit instructions and absorbance at 532 nm was measured using a microplate reader.

3.8. Detection of intracellular iron content

The intracellular ferrous ion (Fe^{2+}) content was measured using the FerroZine iron detection kit. We collected 2×10^6 cells, washed them with PBS, added lysis buffer, and lysed on ice for 10 minutes, then centrifuged and took the supernatant. According to the kit instructions, we added the iron reducer and FerroZine reagent, incubated at room temperature for 15 minutes, and measured the absorbance at 562 nm. The iron concentration (μM/μg protein) was calculated based on the standard curve.

3.9. Glutathione testing

The contents of reduced glutathione (GSH) and oxidized glutathione (GSSG) were measured

using the DTNB recycling method. Cells were collected, 5% metaphosphoric acid was added to precipitate proteins, and after centrifugation, the supernatant was taken to measure total glutathione and GSSG (after derivatization with 2-vinylpyridine). GSH and GSSG concentrations were calculated based on a standard curve, and the GSH/GSSG ratio was used as an indicator of the cellular redox state.

3.10. Protein immunoblotting

After washing the cells with pre-cooled PBS, add RIPA lysis buffer (with protease and phosphatase inhibitors), lyse on ice for 30 minutes, then centrifuge at 4 °C, 12,000×g for 15 minutes and collect the supernatant. After measuring protein concentration using the BCA method, take 30 μg of protein samples for separation by 10% SDS-PAGE and transfer to a PVDF membrane (Millipore). Block with 5% skim milk at room temperature for 1 hour, then add the corresponding primary antibody (1:1000 dilution) and incubate at 4 °C overnight. After washing with TBST, add HRP-conjugated secondary antibody (1:5000) and incubate at room temperature for 1 hour. Develop with ECL chemiluminescence (Bio-Rad ChemiDoc system). Use β-actin as a loading control and perform grayscale analysis with ImageJ software.

3.11. Real-time quantitative PCR

Total RNA was extracted from cells using TRIzol reagent (Invitrogen), and RNA concentration and purity were measured with NanoDrop. 1 μg of RNA was reverse transcribed into cDNA using the PrimeScript RT kit (TaKaRa). Real-time quantitative PCR was performed with SYBR Premix Ex Taq II (TaKaRa) on a QuantStudio 6 Flex system. PCR conditions: 95 °C pre-denaturation for 30 seconds; 95 °C denaturation for 5 seconds, 60 °C annealing/extension for 30 seconds, for 40 cycles. Gapdh was used as the reference gene, and relative expression was calculated using the $2^{-}\Delta\Delta Ct$ method. Primer sequences are shown in Table 1.

Table 1

RT-qPCR primer sequences

Gene	Forward primer (5′–3′)	Reverse primer (5′–3′)
Ifnb1	CCCTATGGAGATGACGGAGA	CTGTCTGCTGGTGGAGTTCA
Cxcl10	CCAAGTGCTGCCGTCATTTT	TCCCTATGGCCCTCATTCTC
Il6	TAGTCCTTCCTACCCCAATTTCC	TTGGTCCTTAGCCACTCCTTC
Tnf	CCCTCACACTCAGATCATCTTCT	GCTACGACGTGGGCTACAG
Gpx4	TGTGCATCCCGCGATGATT	CCTGTACTTATCCAGGCAGA
Slc7a11	GGCACCGTCATCGCATCA	CTCCACAGGCAGACCAGAAA

Acsl4	TCCTGGGAGTGCACTCTGTA	TGGTCTGCTTGGCTCATGTG
Gapdh	AGGTCGGTGTGAACGGATTTG	TGTAGACCATGTAGTTGAGGTCA

3.12. Cytokine testing

The levels of IFN-β, CXCL10/IP-10, IL-6, and TNF-α in the cell culture supernatant were measured using commercial ELISA kits (R&D Systems), following the instructions carefully. Simply put, we added the standards and diluted samples to pre-coated plates, incubated at room temperature for 2 hours, washed, then added the detection antibody and incubated for 1 hour at room temperature. After washing again, we added HRP-conjugated streptavidin, developed the color in the dark, stopped the reaction, and read the absorbance at 450 nm using a plate reader. The concentrations were calculated based on the standard curve.

3.13. Flow cytometry analysis of tumor-infiltrating immune cells

After tumor tissues were dissected and minced, they were digested at 37°C for 45 minutes in RPMI 1640 medium containing 1 mg/mL collagenase IV (Sigma) and 0.1 mg/mL DNase I (Roche). The resulting single-cell suspension was filtered through a 70 μm cell strainer. After removing red blood cells with RBC lysis buffer, the cells were resuspended in PBS containing 2% FBS, incubated on ice for 10 minutes with Fc receptor blocker (anti-CD16/32, clone 93), and then stained with a surface antibody panel (anti-CD45, CD3, CD4, CD8a, CD11c, MHC-II, CD86) at 4°C for 30 minutes in the dark. For intracellular cytokine staining, Brefeldin A (1 μL/mL) and Monensin (2 μM) were added and cells were stimulated at 37°C for 4 hours. After surface staining, cells were fixed and permeabilized (Cytofix/Cytoperm, BD Biosciences), then incubated with anti-IFN-γ and anti-TNF-α antibodies at 4°C for 30 minutes. After washing, data were collected on a BD FACSVerse flow cytometer, and FlowJo software (v10.8) was used to analyze the proportions of immune cell subsets and the expression of activation markers.

3.14. Mouse tumor models and in vivo experiments

Take B16-F10 or MC38 cells in the logarithmic growth phase, digest and wash them, then resuspend in serum-free medium at 1×10^6 cells/100 μL. Inject 100 μL of the cell suspension subcutaneously into the right back of C57BL/6J mice. When the tumor volume reaches about 50-80 mm^3, randomly divide the tumor-bearing mice into groups (5-6 mice per group). The specific treatment plan is as follows: Control group: intratumoral injection of PBS; mtDNA stress induction group: intratumoral injection of TFAM knockdown lentivirus (1×10^9 TU) or intraperitoneal injection of mitochondrial toxic drugs (e.g., oligomycin 2 mg/kg, every other day); ferroptosis induction group: intraperitoneal injection of erastin (20 mg/kg, every other day) or RSL3 (5 mg/kg, every other day);

combined intervention group: co-administration of mtDNA stress inducer and ferroptosis inducer. Measure tumor volume every two days with a caliper and calculate using the formula $V = (\text{length} \times \text{width}^2)/2$. Mice are sacrificed at the experimental endpoint (18-21 days after injection or when tumor diameter reaches 15 mm), tumors are removed and weighed, some tissue is used for flow analysis and histopathological examination, and some is quickly frozen in liquid nitrogen for biochemical and transcriptome analysis.

3.15. Single-cell transcriptome sequencing and analysis

Tumor tissues from the control group and the combined intervention group (3 mice per group, mixed in equal amounts) were collected to prepare single-cell suspensions, and single-cell RNA sequencing was performed using the 10x Genomics Chromium platform. Following the standard procedure, cells were mixed with gel beads and reverse transcription reagents to generate a single-cell emulsion, cDNA libraries were constructed, and paired-end 150 bp sequencing was done on the Illumina NovaSeq 6000 platform, targeting 10,000 cells per sample. The raw data were processed using Cell Ranger (v7.0) for quality control, alignment (reference genome mm10), and expression matrix generation. Downstream analysis was carried out using the Seurat (v4.3) R package: low-quality cells were filtered out (cells with mitochondrial gene percentage >20% or detected genes <200 or >6000 were removed), normalization was done using SCTransform, batch effects were removed with Harmony, and UMAP was used for dimensionality reduction and visualization. Clustering was done with FindClusters (resolution 0.5), and cell types were annotated based on classic marker genes. Differentially expressed genes were identified using FindMarkers, pathway enrichment analysis was performed with GSVA, and cell-cell communication was analyzed with CellChat.

3.16. Statistical analysis

All experiments were independently repeated at least three times, and the data are presented as mean ± standard deviation (mean ± SD). Comparisons between two groups were performed using Student's t-test (unpaired, two-tailed), and comparisons among multiple groups were done using one-way ANOVA followed by Tukey's post hoc test. Survival analysis was carried out using the Kaplan-Meier method and the log-rank test. Statistical analysis was performed with GraphPad Prism 9, and $P < 0.05$ was considered statistically significant.

4. Research Results

4.1. Mitochondrial stress triggers tumor cells to release mtDNA into the cytoplasm and activates the cGAS-STING signaling pathway

To figure out whether mitochondrial stress can trigger the release of mtDNA into the cytoplasm

and activate innate immune sensing, we first induced mitochondrial stress in B16-F10 and MC38 cells in three ways: using mitochondrial oxidative phosphorylation inhibitors oligomycin/antimycin A (O/A), the mitochondrial uncoupler CCCP, and knocking down the TFAM gene. Extracting cytoplasmic DNA and performing qPCR showed that all three treatments significantly increased cytoplasmic mtDNA copies (Figure 1A,Table 1A), suggesting that mitochondrial stress can promote mtDNA escape into the cytoplasm. Next, Western blot analysis showed that O/A treatment and TFAM knockdown both time-dependently upregulated phosphorylation at STING Ser365, TBK1 Ser172, and IRF3 Ser396 (Figures 1B and 1C,Table 1B,Table 1C), indicating activation of the cGAS-STING pathway. Consistently, RT-qPCR results found that mitochondrial stress significantly induced mRNA expression of downstream interferon-stimulated genes Ifnb1 and the chemokine Cxcl10 (Figure 1D,Table 1D). ELISA further confirmed that IFN-β and CXCL10 protein secretion levels in the culture supernatant were notably increased (Figure 1E,Table 1E). Interestingly, in B16-F10 cells with cGAS or STING knocked out, the upregulation of Ifnb1 and Cxcl10 induced by mitochondrial stress was completely blocked (Figure 1F,Table 1F), proving that this process relies on the cGAS-STING axis. Overall, these results show that mtDNA release into the cytoplasm caused by mitochondrial stress can effectively trigger innate immune signaling in tumor cells.

Figure 1

A: Cytosolic mtDNA copies after mitochondrial stress

B: Time course of STING/TBK1 phosphorylation after O/A treatment

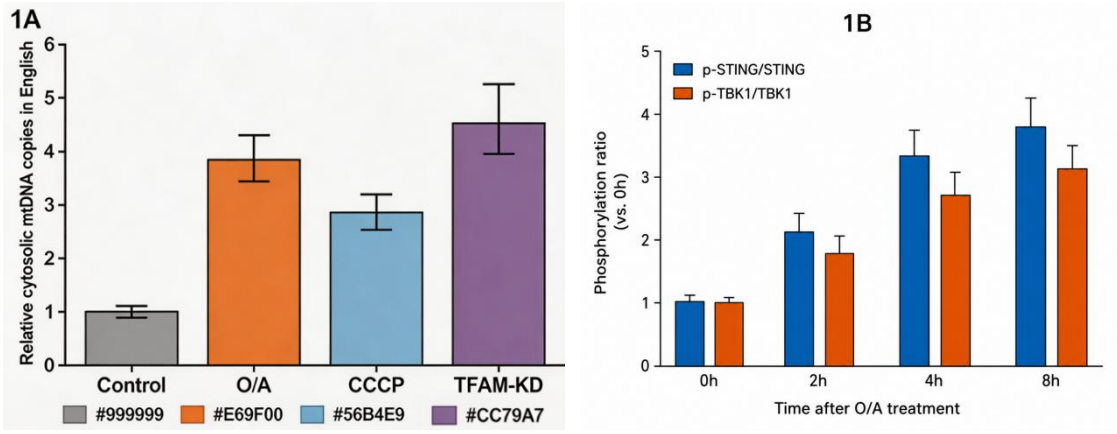

C: Phosphorylation levels in TFAM-KD vs Control

Global Health Care
WISDOM ACADEMIC https://doi.org/10.63808/ghc.v2i1.524 Volume 2 , Issue 1

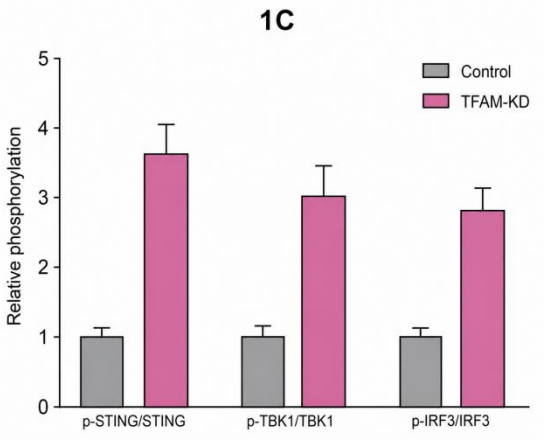

D: mRNA expression of Ifnb1 and Cxcl10 after mitochondrial stress

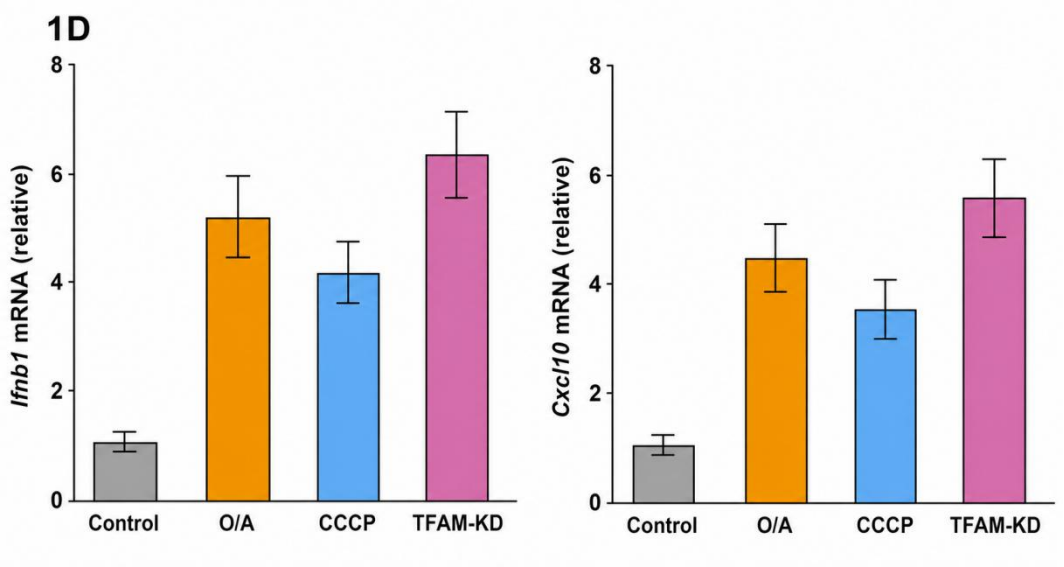

E: ELISA for IFN-β and CXCL10 secretion

F: cGAS-KO and STING-KO block Ifnb1/Cxcl10 induction after O/A

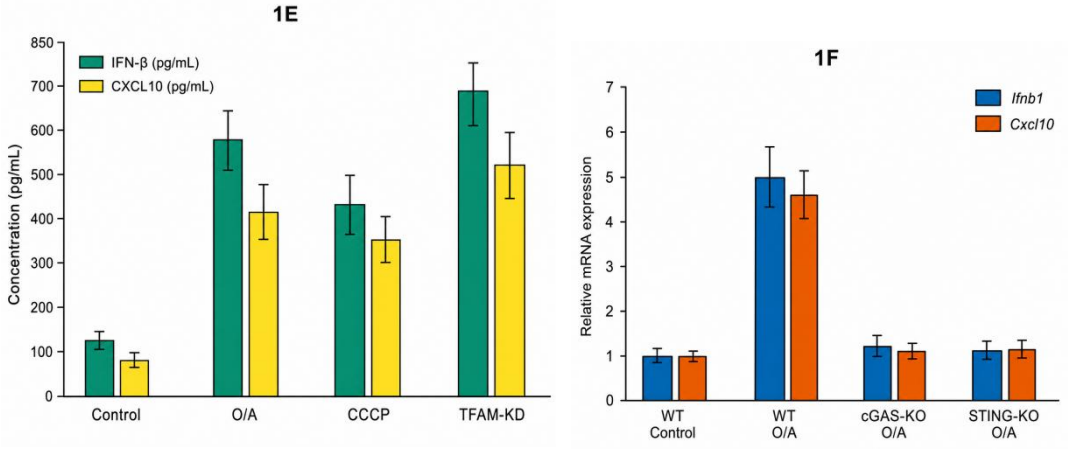

Table 1A: Cytosolic mtDNA copies after mitochondrial stress

Group	Relative mtDNA copy number
Control	1.00 ± 0.15

O/A	3.80 ± 0.45
CCCP	2.90 ± 0.38
TFAM-KD	4.50 ± 0.52

Table 1B: Time course of STING/TBK1 phosphorylation after O/A treatment

Time	p-STING/STING	p-TBK1/TBK1
0h	1.00 ± 0.12	1.00 ± 0.10
2h	2.10 ± 0.25	1.80 ± 0.22
4h	3.30 ± 0.40	2.70 ± 0.32
8h	3.80 ± 0.45	3.10 ± 0.38

Table 1C: Phosphorylation levels in TFAM-KD vs Control

protein	Comparison	TFAM-KD
p-STING/STING	1.00 ± 0.10	3.60 ± 0.40
p-TBK1/TBK1	1.00 ± 0.12	3.00 ± 0.35
p-IRF3/IRF3	1.00 ± 0.10	2.80 ± 0.32

Table 1D: mRNA expression of Ifnb1 and Cxcl10 after mitochondrial stress

Group	Ifnb1	Cxcl10
Control	1.00 ± 0.20	1.00 ± 0.18
O/A	5.20 ± 0.70	4.40 ± 0.55
CCCP	4.10 ± 0.60	3.50 ± 0.50
TFAM-KD	6.30 ± 0.80	5.60 ± 0.65

Table 1E: ELISA for IFN-β and CXCL10 secretion

Group	IFN-β	CXCL10
Control	120 ± 20	80 ± 12
O/A	580 ± 70	410 ± 60
CCCP	430 ± 55	350 ± 48
TFAM-KD	690 ± 80	520 ± 70

Table 1F: cGAS-KO and STING-KO block Ifnb1/Cxcl10 induction after O/A

Group	Ifnb1	Cxcl10
WT Control	1.00 ± 0.15	1.00 ± 0.12

WT O/A	5.00 ± 0.65	4.60 ± 0.55
cGAS-KO O/A	1.20 ± 0.20	1.10 ± 0.18
STING-KO O/A	1.10 ± 0.18	1.15 ± 0.16

4.2. Activation of the cGAS-STING pathway promotes ferroptosis in tumor cells

Since the core feature of ferroptosis is iron-dependent lipid peroxidation, we further tested how cGAS-STING activation affects tumor cell sensitivity to ferroptosis. B16-F10 and MC38 cells were treated with the STING agonist cGAMP (10 μg/mL) for 24 hours, and lipid peroxidation levels were measured using the C11-BODIPY probe. The results showed that cGAMP treatment increased the mean fluorescence intensity (MFI) of oxidized C11-BODIPY by about 3-4 times compared to the control group (Figure 2A,Table 2A), indicating a significant accumulation of lipid peroxides. At the same time, intracellular malondialdehyde (MDA) content increased significantly, ferrous ion (Fe^{2+}) levels went up, and the reduced/oxidized glutathione ratio (GSH/GSSG) dropped significantly (Table 2), showing typical biochemical features of ferroptosis. However, in STING knockout (Tmem173-KO) cells, these cGAMP-induced changes in ferroptosis markers almost disappeared (Figure 2B, Table 2,Table 2B). Similarly, in cGAS knockout cells, treatment with the mitochondrial stress inducer O/A also failed to effectively trigger lipid peroxidation (Figure 2C,Table 2C). Importantly, the ferroptosis inhibitor ferrostatin-1 (Fer-1, 2 μM) and the iron chelator deferoxamine (DFO, 100 μM) completely blocked cGAMP-induced lipid peroxidation and cell death (Figures 2D, 2E,Table 2D,2E) but did not affect STING phosphorylation levels (Figure 2F,Table 2F), indicating that STING activation occurs upstream of the ferroptosis events. Taken together, these results suggest that activating the cGAS-STING pathway is enough to induce ferroptosis in tumor cells.

Figure 2

A: cGAMP induces lipid peroxidation (C11-BODIPY MFI)

B: STING-KO abolishes cGAMP-induced lipid peroxidation

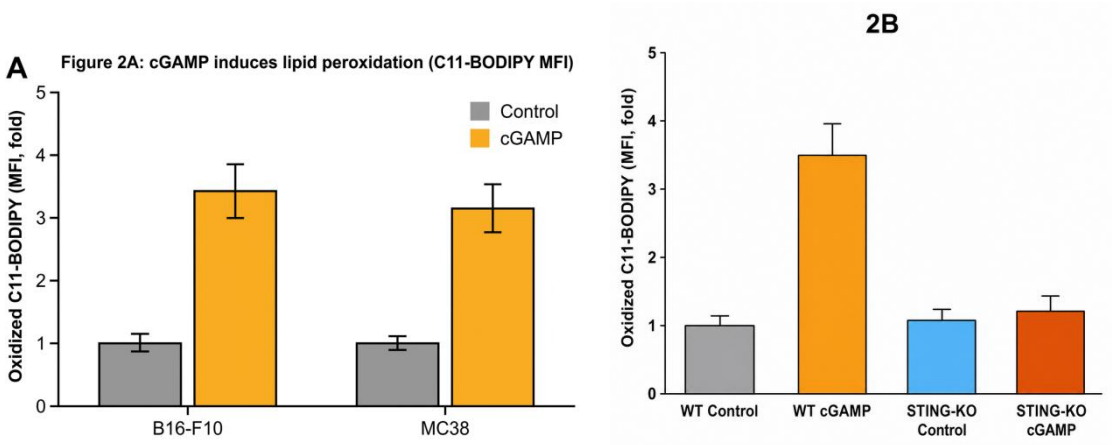

C: cGAS-KO blocks O/A-induced lipid peroxidation

D: Fer-1 and DFO inhibit cGAMP-induced cell death

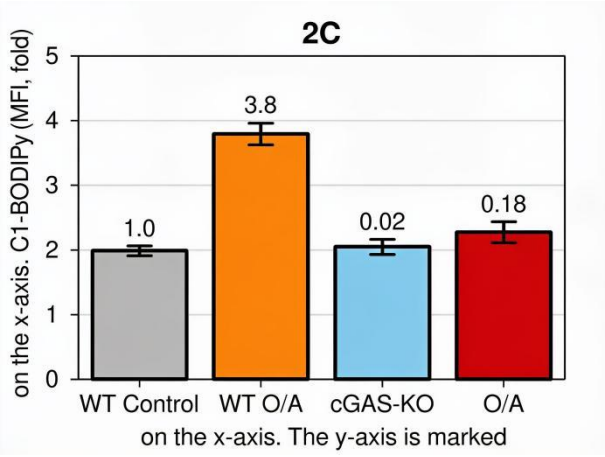

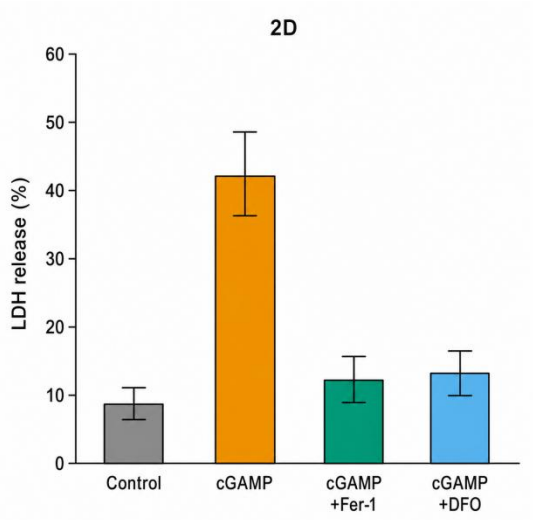

E: Fer-1 and DFO inhibit cGAMP-induced lipid peroxidation

F: Fer-1 does not affect STING phosphorylation induced by cGAMP

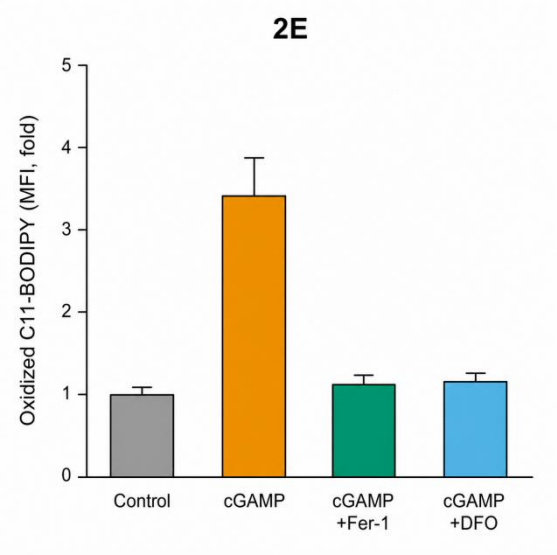

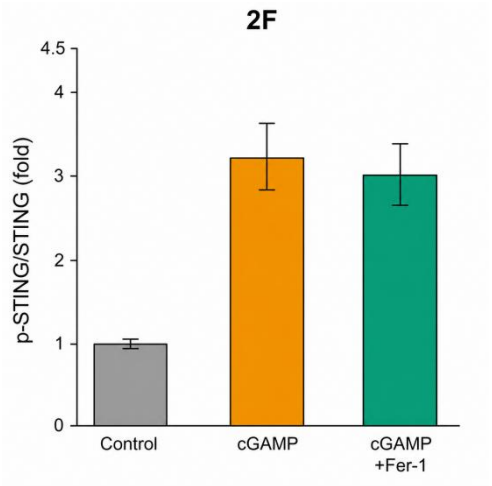

Table 2

Effects of cGAMP treatment on ferroptosis-related markers in B16-F10 cells (mean ± SD, n = 3)

Treatment group	MDA (nmol/mg protein)	Fe^{2+} (μM/μg protein)	GSH/GSSG ratio	Oxidized C11-BODIPY (MFI)
Contrast	1.25 ± 0.18	0.42 ± 0.06	8.73 ± 1.02	1.00 ± 0.12
cGAMP	3.86 ± 0.45	1.15 ± 0.14	2.91 ± 0.38	3.42 ± 0.41
cGAMP + Fer-1	1.31 ± 0.21	1.08 ± 0.12	7.85 ± 0.93	1.12 ± 0.15
cGAMP + DFO	1.42 ± 0.19	0.55 ± 0.07	7.54 ± 0.88	1.08 ± 0.14
Tmem173-KO + cGAMP	1.28 ± 0.16	0.48 ± 0.09	8.19 ± 1.05	1.06 ± 0.13

Note. B16-F10 cells were analyzed 24 hours after the specified treatment. Oxidized C11-BODIPY was normalized to the MFI of the control group. Fer-1: ferrostatin-1 (2 μM); DFO: deferoxamine (100 μM). Tmem173-KO: STING knockout cells.

Table 2A: cGAMP induces lipid peroxidation (C11-BODIPY MFI)

Cell line	control group	cGAMP group
B16-F10	1.00 ± 0.12	3.42 ± 0.41
MC38	1.00 ± 0.10	3.15 ± 0.38

Table 2B: STING-KO abolishes cGAMP-induced lipid peroxidation

Group	MFI Relative Multiple
WT Control	1.00 ± 0.11
WT cGAMP	3.50 ± 0.42
STING-KO Control	1.05 ± 0.12
STING-KO cGAMP	1.20 ± 0.15

Table 2C: cGAS-KO blocks O/A-induced lipid peroxidation

Group	MFI Relative Multiple
WT Control	1.00 ± 0.12
WT O/A	3.80 ± 0.48
cGAS-KO Control	1.02 ± 0.13
cGAS-KO O/A	1.30 ± 0.18

Table 2D: Fer-1 and DFO inhibit cGAMP-induced cell death

Group	LDH release rate
Control	8.5 ± 2.1
cGAMP	42.3 ± 5.6
cGAMP + Fer-1	12.1 ± 2.8
cGAMP + DFO	13.4 ± 3.0

Table 2E: Fer-1 and DFO inhibit cGAMP-induced lipid peroxidation

Group	MFI Relative Multiple
Control	1.00 ± 0.11
cGAMP	3.40 ± 0.40

cGAMP + Fer-1	1.10 ± 0.13
cGAMP + DFO	1.15 ± 0.14

Table 2F: Fer-1 does not affect STING phosphorylation induced by cGAMP

Group	p-STING/STING
Control	1.00 ± 0.12
cGAMP	3.20 ± 0.38
cGAMP + Fer-1	3.00 ± 0.35

4.3. cGAS-STING activation induces ferroptosis by downregulating the xCT/GPX4 antioxidant axis

To figure out how STING activation triggers ferroptosis at the molecular level, we looked at changes in the key ferroptosis-related proteins. Western blot results showed that cGAMP treatment significantly reduced the protein levels of xCT (SLC7A11) and GPX4 in a dose- and time-dependent manner (Figure 3A and 3B,Table 3A,Table 3B), while increasing the expression of the pro-ferroptotic protein ACSL4. RT-qPCR analysis indicated that the mRNA levels of Slc7a11 and Gpx4 dropped significantly just 4 hours after cGAMP treatment (Figure 3C,Table 3C), suggesting that the STING pathway suppresses the antioxidant axis at the transcription level. Using an IRF3-specific inhibitor or IRF3 siRNA could partially reverse cGAMP's downregulation of Slc7a11 and Gpx4 (Figure 3D,Table 3D), while an NF-κB inhibitor had no noticeable effect, indicating that this process mainly relies on the IRF3 signaling branch. Functionally, overexpressing SLC7A11 or GPX4 via lentivirus significantly restored intracellular GSH levels and blocked cGAMP-induced lipid peroxidation and cell death (Figure 3E and 3F,Table 3E,Table 3F), whereas the control empty vector offered no protection. Altogether, these data suggest that the cGAS-STING-IRF3 signaling axis disrupts tumor cell redox balance and promotes ferroptosis by transcriptionally suppressing the xCT/GPX4 antioxidant system.

Figure 3

A: cGAMP dose-dependent downregulation of xCT and GPX4 (simulated Western blot quantification)

B: Time course of protein changes after cGAMP (10 μg/mL)

Global Health Care
WISDOM ACADEMIC https://doi.org/10.63808/ghc.v2i1.524 Volume 2 , Issue 1

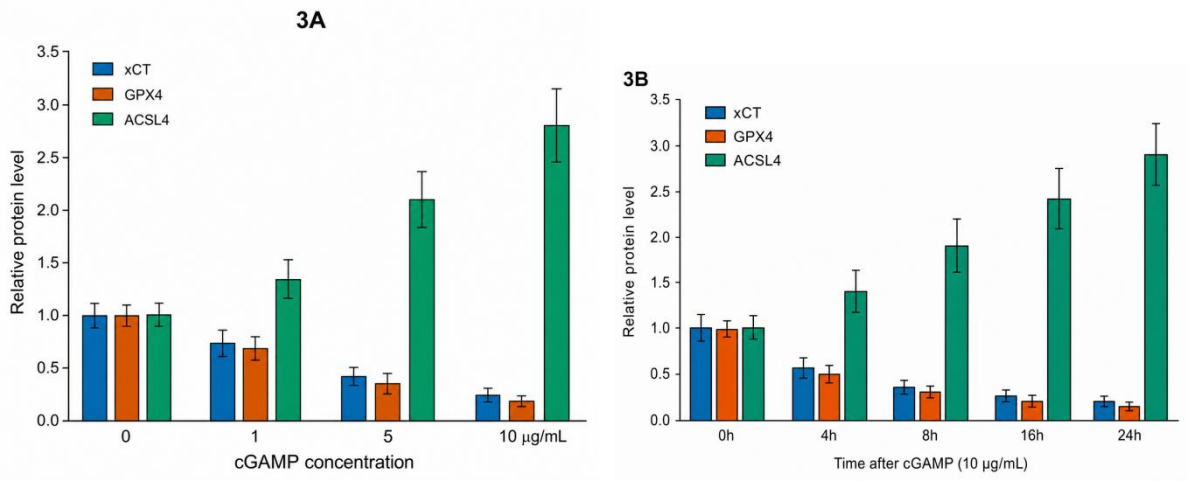

C: mRNA levels of Slc7a11 and Gpx4 after cGAMP treatment

D: IRF3 inhibition reverses cGAMP-induced downregulation of Slc7a11/Gpx4

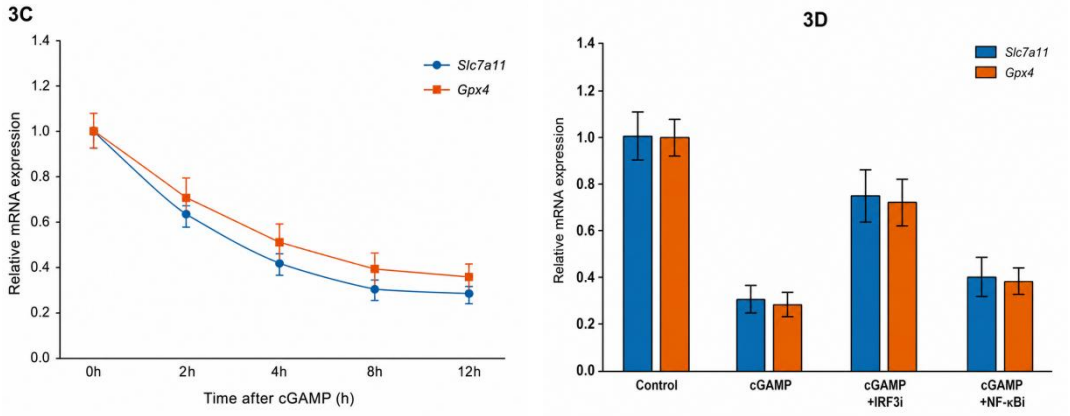

E: Overexpression of SLC7A11 or GPX4 restores GSH levels

F: Overexpression of SLC7A11/GPX4 blocks cGAMP-induced cell death

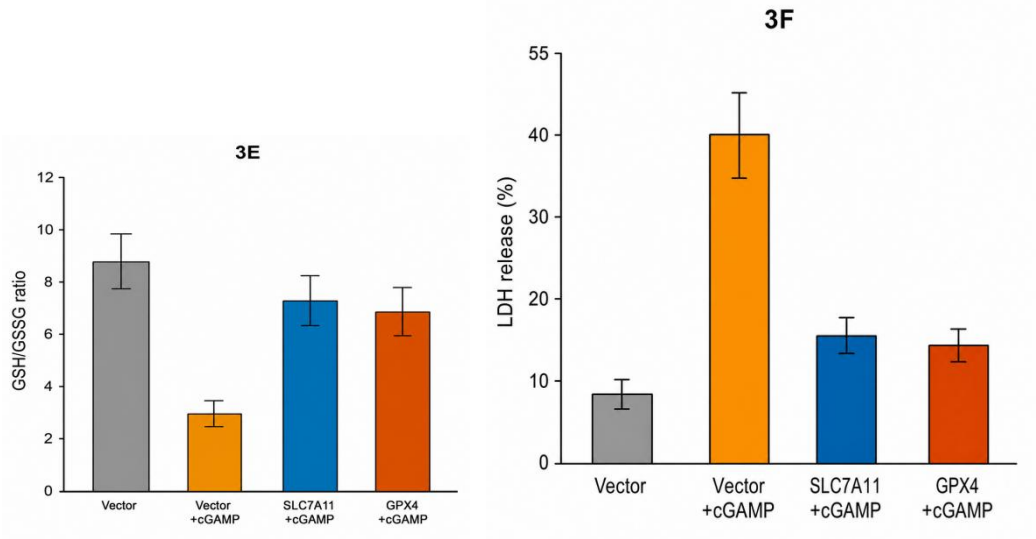

Table 3A: cGAMP dose-dependent downregulation of xCT and GPX4 (simulated Western blot quantification)

Concentration (μg/mL)	xCT	GPX4	ACSL4
0	1.00 ± 0.08	1.00 ± 0.07	1.00 ± 0.10
1	0.72 ± 0.09	0.68 ± 0.08	1.35 ± 0.15
5	0.41 ± 0.06	0.35 ± 0.06	2.10 ± 0.22
10	0.22 ± 0.05	0.18 ± 0.04	2.80 ± 0.30

Table 3B: Time course of protein changes after cGAMP (10 μg/mL)

Time (h)	xCT	GPX4	ACSL4
0	1.00 ± 0.08	1.00 ± 0.07	1.00 ± 0.10
4	0.55 ± 0.07	0.50 ± 0.06	1.40 ± 0.18
8	0.35 ± 0.05	0.30 ± 0.05	1.90 ± 0.22
16	0.25 ± 0.04	0.20 ± 0.04	2.40 ± 0.28
24	0.20 ± 0.04	0.15 ± 0.03	2.90 ± 0.32

Table 3C: mRNA levels of Slc7a11 and Gpx4 after cGAMP treatment

Time (h)	Slc7a11	Gpx4
0	1.00 ± 0.08	1.00 ± 0.07
2	0.65 ± 0.09	0.70 ± 0.08
4	0.42 ± 0.06	0.50 ± 0.07
8	0.30 ± 0.05	0.38 ± 0.06
12	0.28 ± 0.05	0.35 ± 0.05

Table 3D: IRF3 inhibition reverses cGAMP-induced downregulation of Slc7a11/Gpx4

Group	Slc7a11	Gpx4
Control	1.00 ± 0.08	1.00 ± 0.07
cGAMP	0.30 ± 0.05	0.28 ± 0.04
cGAMP + IRF3i	0.75 ± 0.10	0.72 ± 0.09
cGAMP + NF-κBi	0.40 ± 0.06	0.38 ± 0.05

Table 3E: Overexpression of SLC7A11 or GPX4 restores GSH levels

Group	GSH/GSSG ratio
Empty vector control	8.70 ± 1.00
empty carrier+ cGAMP	2.90 ± 0.40

SLC7A11 OE + cGAMP	7.20 ± 0.90
GPX4 OE + cGAMP	6.80 ± 0.85

Table 3F: Overexpression of SLC7A11/GPX4 blocks cGAMP-induced cell death

Group	LDH release rate
Empty carrier control	8.2 ± 2.0
Empty carrier + cGAMP	40.5 ± 5.2
SLC7A11 OE + cGAMP	15.3 ± 2.5
GPX4 OE + cGAMP	14.1 ± 2.3

4.4. The mtDNA-cGAS-STING axis forms a positive feedback loop with ferroptosis

The results above show a one-way signaling path from mtDNA → cGAS-STING → ferroptosis. We then explored whether ferroptosis could, in turn, promote mtDNA release and STING activation, forming a positive feedback loop. Treating B16-F10 cells with classic ferroptosis inducers erastin (5 μM) or RSL3 (1 μM) for 12 hours led to a significant increase in cytoplasmic mtDNA copies (Fig. 4A,Table 4A), along with obvious upregulation of STING and TBK1 phosphorylation levels (Fig. 4B,Table 4B). This effect could be completely blocked by pre-treating with the ferroptosis inhibitor Fer-1, but not by the apoptosis inhibitor zVAD-fmk or the necroptosis inhibitor necrostatin-1 (Fig. 4C,Table 4C), suggesting that ferroptosis itself specifically drives mtDNA release. More importantly, in STING knockout cells, erastin-induced mtDNA release still occurred, but the downstream expression of Ifnb1 and Cxcl10 was significantly reduced (Fig. 4D,Table 4D), indicating that mtDNA generated from ferroptosis is sensed by STING to amplify the innate immune signal. At the same time, compared with wild-type cells, STING knockout cells were more resistant to erastin-induced lipid peroxidation and cell death (Fig. 4E, 4F,Table 4E,4F), showing that STING-mediated signaling feedback strengthens the ferroptosis process. In short, the mtDNA-cGAS-STING pathway and ferroptosis form a self-amplifying positive feedback loop: STING activation promotes ferroptosis, and ferroptosis, in turn, releases more mtDNA to further activate STING, boosting immune stimulation.

Figure 4

A: Ferroptosis inducers increase cytosolic mtDNA

B: Ferroptosis inducers activate STING/TBK1

Global Health Care
WISDOM ACADEMIC https://doi.org/10.63808/ghc.v2i1.524 Volume 2 , Issue 1

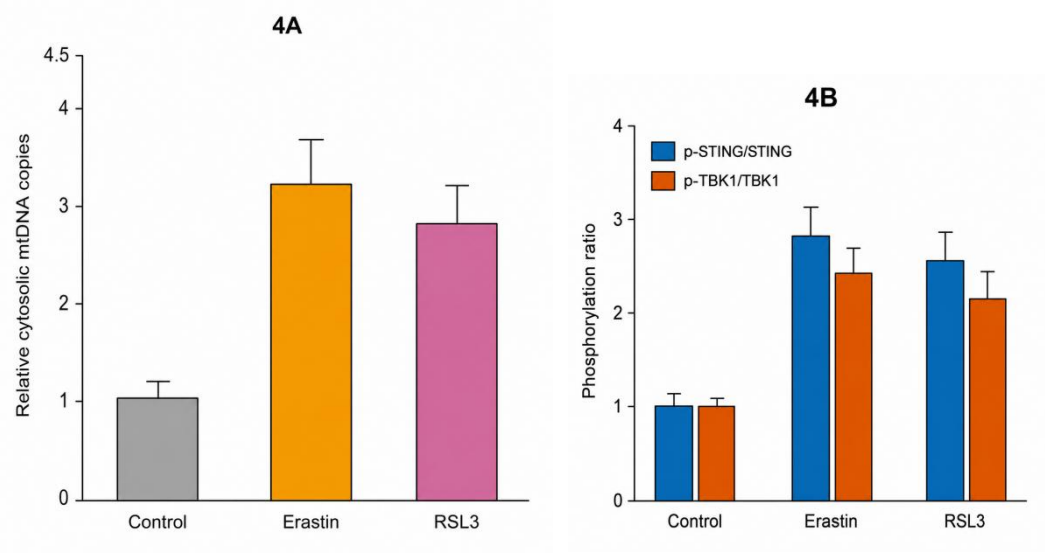

C: Fer-1 specifically inhibits erastin-induced mtDNA release

D: STING-KO reduces erastin-induced Ifnb1/Cxcl10 expression

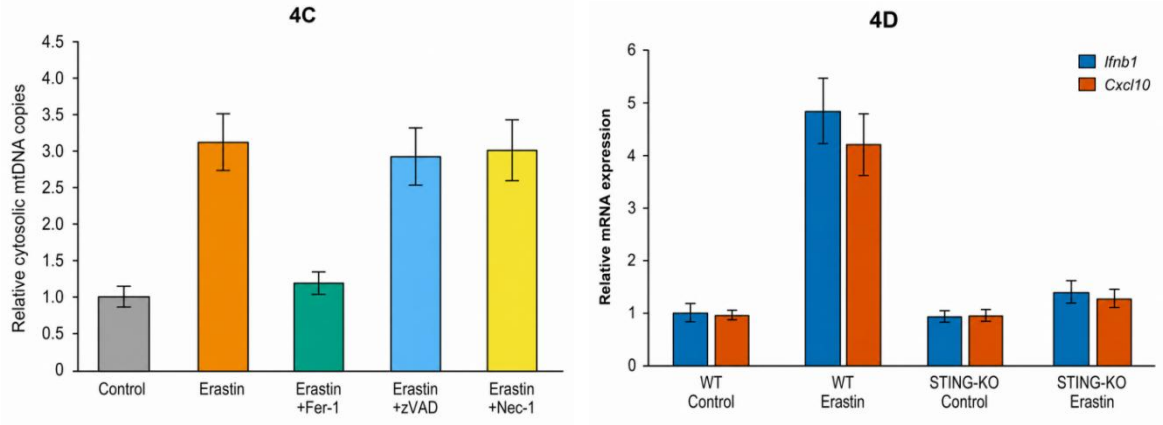

E: STING-KO confers resistance to erastin-induced lipid peroxidation

F: STING-KO reduces erastin-induced cell death

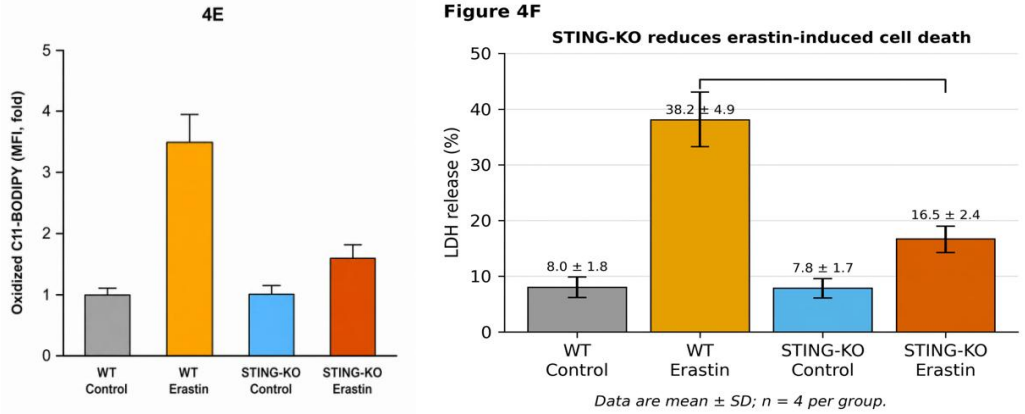

Table 4A: Ferroptosis inducers increase cytosolic mtDNA

Group	Relative mtDNA copy number
Control	1.00 ± 0.15

Erastin	3.20 ± 0.40
RSL3	2.80 ± 0.35

Table 4B: Ferroptosis inducers activate STING/TBK1

Group	p-STING/STING	p-TBK1/TBK1
Control	1.00 ± 0.12	1.00 ± 0.10
Erastin	2.80 ± 0.35	2.40 ± 0.30
RSL3	2.50 ± 0.30	2.10 ± 0.27

Table 4C: Fer-1 specifically inhibits erastin-induced mtDNA release

Group	Relative mtDNA copy number
Control	1.00 ± 0.13
Erastin	3.10 ± 0.38
Erastin + Fer-1	1.20 ± 0.16
Erastin + zVAD	2.90 ± 0.35
Erastin + Nec-1	3.00 ± 0.37

Table 4D: STING-KO reduces erastin-induced Ifnb1/Cxcl10 expression

Group	Ifnb1	Cxcl10
WT Control	1.00 ± 0.14	1.00 ± 0.12
WT Erastin	4.80 ± 0.60	4.20 ± 0.55
STING-KO Control	0.90 ± 0.12	0.95 ± 0.13
STING-KO Erastin	1.40 ± 0.18	1.30 ± 0.16

Table 4E: STING-KO confers resistance to erastin-induced lipid peroxidation

Group	MFI Relative Multiple
WT Control	1.00 ± 0.11
WT Erastin	3.50 ± 0.42
STING-KO Control	1.03 ± 0.12
STING-KO Erastin	1.60 ± 0.20

Table 4F: STING-KO reduces erastin-induced cell death

Group	LDH release rate
WT Control	8.0 ± 1.8

WT Erastin	38.2 ± 4.9
STING-KO Control	7.8 ± 1.7
STING-KO Erastin	16.5 ± 2.4

4.5. Joint induction of mtDNA release and ferroptosis synergistically enhances tumor immune microenvironment remodeling

To evaluate the impact of mtDNA sensing combined with ferroptosis on the tumor immune microenvironment, we treated B16-F10 syngeneic tumor models with either TFAM knockdown lentivirus (to induce mtDNA release), erastin (to induce ferroptosis), or a combination of both. Tumor tissues were collected on day 10 of treatment for single-cell RNA sequencing (scRNA-seq). Cell clustering analysis identified multiple cell subtypes including tumor cells, T cells, NK cells, macrophages, dendritic cells (DCs), fibroblasts, and others (Figure 5A). UMAP visualization showed that compared to the control and single-drug groups, the combination treatment group had a significant increase in $CD8^+$ T cells and mature DCs (high Cd86 and MHC-II expression), while the proportion of immunosuppressive tumor-associated macrophages (high Arg1 expression) and regulatory T cells decreased (Figure 5B,Table 5A). Differential gene expression and pathway enrichment analysis revealed that cytotoxic effector molecules (Gzmb, Prf1) and activation markers (Ifng, Tnf) were significantly upregulated in tumor-infiltrating $CD8^+$ T cells in the combination group (Figure 5C,Table 5B). CellChat intercellular communication analysis indicated that the combination treatment enhanced antigen presentation and costimulatory signaling between DCs and $CD8^+$ T cells (Figure 5D,Table 5C).

Figure 5

A: UMAP visualization of scRNA-seq clusters

B: Changes in cell subset proportions after treatment

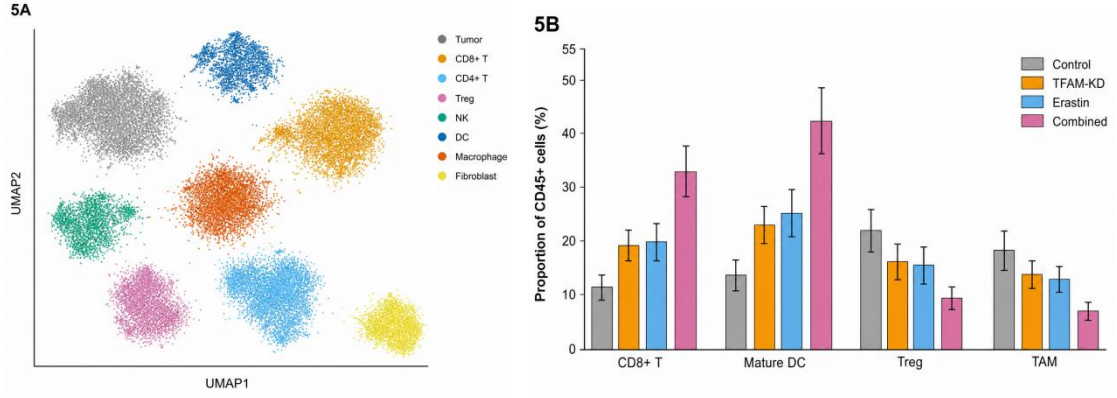

C: Expression of effector genes in CD8+ T cells (heatmap)

D: CellChat interaction strength between DC and CD8+ T cells

Global Health Care
WISDOM ACADEMIC https://doi.org/10.63808/ghc.v2i1.524 Volume 2 , Issue 1

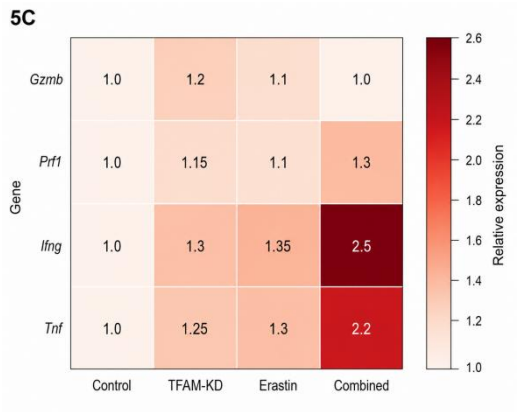

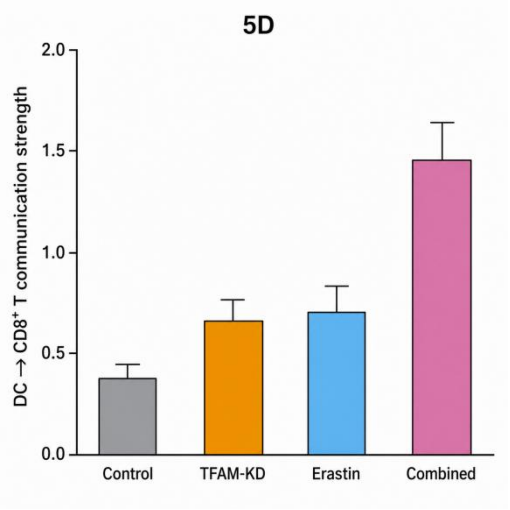

Table 5A: Changes in cell subset proportions after treatment

Indicator	Control	TFAM-KD	Erastin	Combined
$CD8^+$ T cell	11.2 ± 1.8	18.6 ± 2.5	19.3 ± 2.7	32.4 ± 4.1
$CD86^+MHC\text{-}II^+$ DC	13.4 ± 2.1	22.8 ± 3.0	25.1 ± 3.4	41.7 ± 5.3
IFN-γ^+TNF-α^+ $CD8^+$ T cell	8.6 ± 1.3	15.2 ± 2.2	16.9 ± 2.5	29.3 ± 3.8
Regulatory T cells (part of $CD4^+$)	21.5 ± 2.9	16.3 ± 2.0	15.8 ± 2.4	9.6 ± 1.7
Tumor-associated macrophages ($Arg1^+$)	18.4 ± 2.6	13.7 ± 2.1	12.9 ± 1.8	7.2 ± 1.3

Table 5B: Expression of effector genes in CD8+ T cells (heatmap)

Gene	Control	TFAM-KD	Erastin	Combined
Gzmb	1.00	1.20	1.10	1.00
Prf1	1.00	1.15	1.10	1.30
Ifng	1.00	1.30	1.35	2.50
Tnf	1.00	1.25	1.30	2.20

Table 5C: CellChat interaction strength between DC and CD8+ T cells

Group	Signal Strength
Control	0.35 ± 0.06
TFAM-KD	0.62 ± 0.09
Erastin	0.68 ± 0.10
Combined	1.45 ± 0.18

Flow cytometry quantification further supported the above results (Table 3): the proportion of $CD8^+$ T cells among tumor-infiltrating $CD45^+$ cells in the combination treatment group increased to

(32.4 ± 4.1)%, significantly higher than the control group (11.2 ± 1.8%) and the single-drug groups (TFAM-KD: 18.6 ± 2.5%; erastin: 19.3 ± 2.7%). At the same time, the proportion of $CD86^+MHC\text{-}II^+$ mature DCs in the combination group reached (41.7 ± 5.3)%, about three times that of the control group. Functional cytokine testing showed that the proportion of $IFN\text{-}\gamma^+TNF\text{-}\alpha^+$ double-positive cells among tumor-infiltrating $CD8^+$ T cells was significantly increased in the combination group (Table 3). These results suggest that mtDNA-cGAS-STING activation and ferroptosis together reshape the tumor immune microenvironment in vivo, promoting the recruitment and activation of effector T cells.

Table 3

Proportions of tumor-infiltrating immune cells in B16-F10 under different treatments (mean ± SD, n = 5–6)

Indicator	control group	TFAM-KD group	Erastin group	Combined treatment group
$CD8^+$ T cells (as a percentage of $CD45^+$)	11.2 ± 1.8	18.6 ± 2.5	19.3 ± 2.7	32.4 ± 4.1
$CD86^+MHC\text{-}II^+$ DC (as a percentage of $CD45^+$)	13.4 ± 2.1	22.8 ± 3.0	25.1 ± 3.4	41.7 ± 5.3
$IFN\text{-}\gamma^+TNF\text{-}\alpha^+$ $CD8^+$ T cells (%)	8.6 ± 1.3	15.2 ± 2.2	16.9 ± 2.5	29.3 ± 3.8
Regulatory T cells (as a percentage of $CD4^+$)	21.5 ± 2.9	16.3 ± 2.0	15.8 ± 2.4	9.6 ± 1.7
Tumor-associated macrophages ($Arg1^+$, % of $CD45^+$)	18.4 ± 2.6	13.7 ± 2.1	12.9 ± 1.8	7.2 ± 1.3

Note. C57BL/6J mice were subcutaneously injected with B16-F10 cells, and when the tumor volume reached about 60 mm^3, they received an intratumoral injection of TFAM knockdown lentivirus (1×10^9 TU, single dose) and/or intraperitoneal injection of erastin (20 mg/kg, every other day). Samples were collected on day 10 of treatment for flow cytometry analysis. Compared with the control group, $P < 0.05$, $P < 0.001$; compared with the single drug groups, the combination group had $P < 0.05$.

4.6. Combined treatment significantly inhibits tumor growth in the body and extends survival

Finally, we evaluated the in vivo contribution of co-activation of mtDNA-cGAS-STING axis and ferroptosis on tumor treatment efficacy. In two homologous transplant tumor models, B16-F10 melanoma and MC38 colon cancer, tumor-bearing mice received PBS control, TFAM knockdown lentivirus (intratumoral injection), erastin (intraperitoneal injection), or combination therapy, respectively. As shown in Figures 6A and 6B(Table 6A,6B), monotherapy can delay tumor growth to some extent, but tumor volume in the combination group was significantly smaller than in the monotherapy group throughout the observation period. Tumor weight statistics at the treatment

endpoint (day 18 post-vaccination) showed that the combined group in the B16-F10 model had an average tumor weight reduction of about 78% compared to the control group (Figure 6C,Table 6C), about 55% less than the TFAM-KD group, and about 52% less than the Elastin group; The MC38 model showed consistent trends in results (Figure 6D,Table 6D). Survival analysis showed that combination therapy significantly extended mouse survival (Figures 6E, 6F,Table 6E,6F), with median survival in the combination group of 38 days in the B16-F10 model versus 21 days in the control group (log-rank test, $P < 0.001$). Notably, in STING knockout B16-F10 tumors, the inhibitory effect on tumor growth of combination therapy was significantly reduced (Figure 6G,Table 6G), and intratumoral $CD8^+$ T cell infiltration was also significantly reduced compared to the wild-type combination group (Figure 6H,Table 6H), further confirming that this synergistic antitumor effect depends on host STING signaling. In summary, in vivo experiments have shown that combined induction of mtDNA release and ferroptosis synergistically remodels the tumor immune microenvironment by activating the cGAS-STING pathway, thereby effectively inhibiting tumor growth and prolonging survival in tumor-bearing mice.

Figure 6

A: B16-F10 tumor growth curves

B: MC38 tumor growth curves

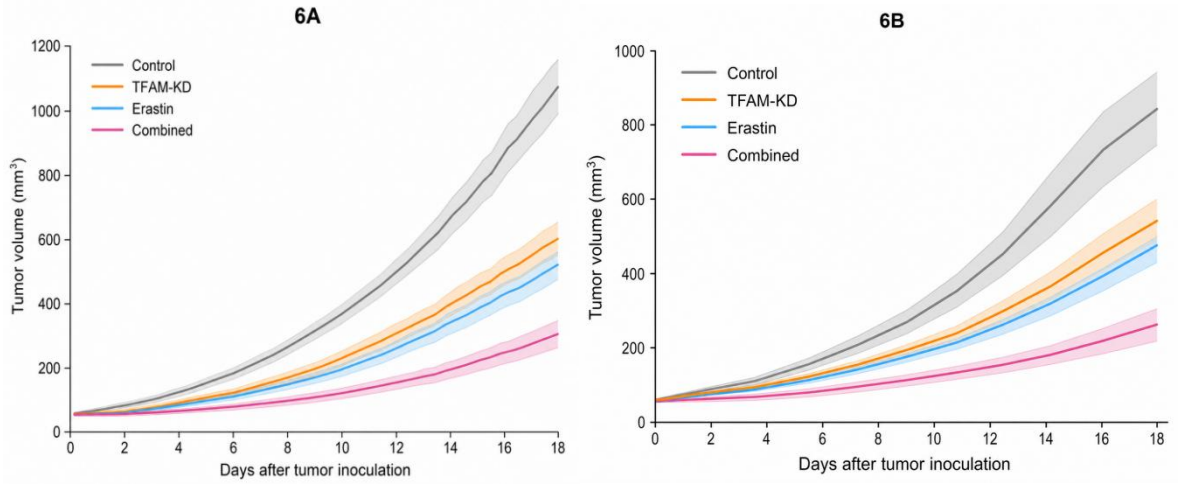

C: B16-F10 endpoint tumor weights

D: MC38 endpoint tumor weights

https://doi.org/10.63808/ghc.v2i1.524 Volume 2 , Issue 1

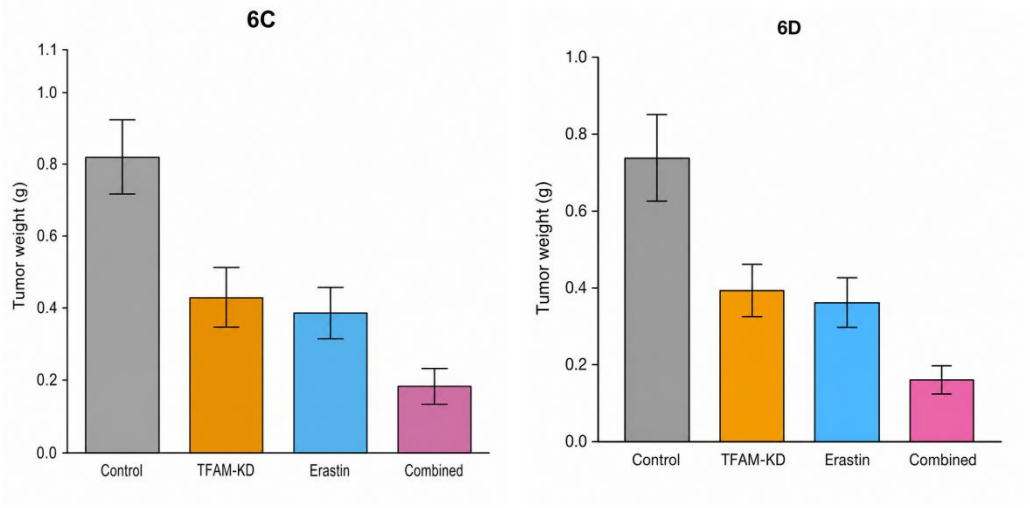

E: B16-F10 survival curves (Kaplan-Meier)

F: MC38 survival curves

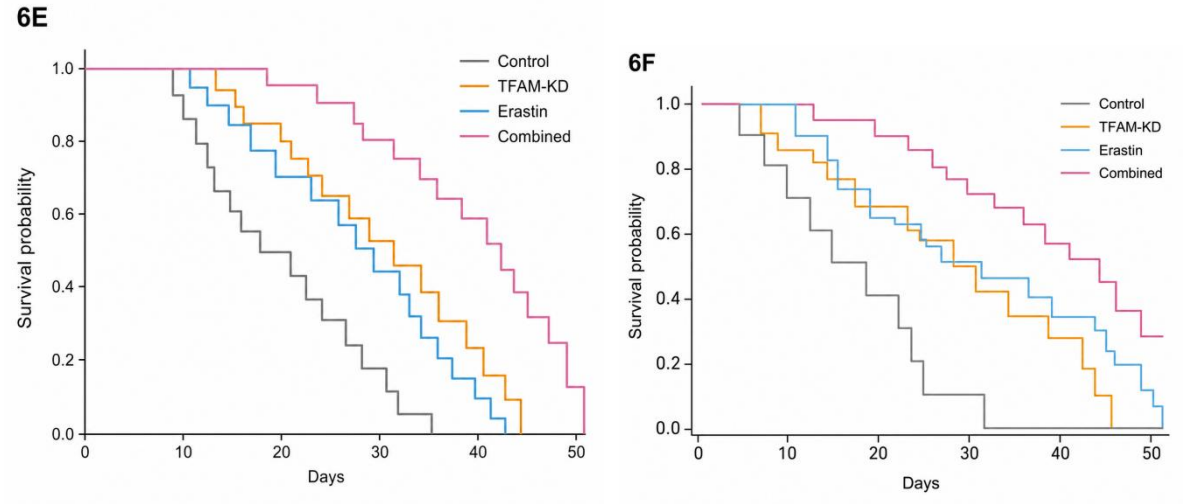

G: STING-KO tumor growth with combined treatment

H: CD8+ T cell infiltration in STING-KO tumors after combined treatment

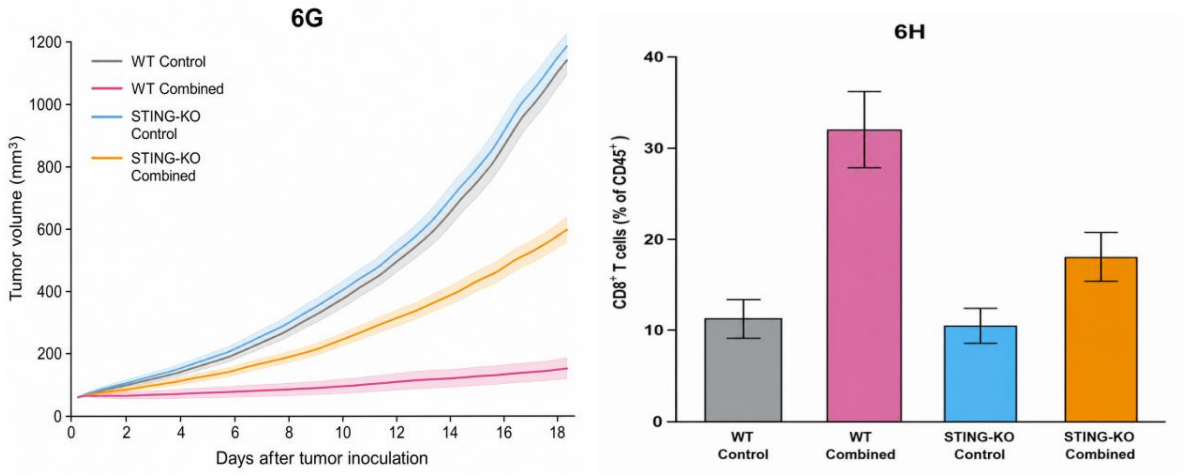

Table 6A: B16-F10 tumor growth curves

Days	Control	TFAM-KD	Erastin	Combined
0	60 ± 6	60 ± 6	60 ± 6	60 ± 6
2	86 ± 9	78 ± 8	80 ± 8	65 ± 7
4	124 ± 14	98 ± 11	102 ± 12	72 ± 8
6	178 ± 20	124 ± 14	130 ± 15	80 ± 9
8	255 ± 29	156 ± 18	164 ± 19	90 ± 10
10	365 ± 42	196 ± 22	207 ± 24	102 ± 12
12	523 ± 60	246 ± 28	261 ± 30	116 ± 14
14	749 ± 86	309 ± 36	329 ± 38	133 ± 16
16	1073 ± 123	388 ± 45	414 ± 48	153 ± 18
18	1537 ± 176	487 ± 56	521 ± 61	176 ± 21

Table 6B: MC38 tumor growth curves

Days	Control	TFAM-KD	Erastin	Combined
0	60 ± 6	60 ± 6	60 ± 6	60 ± 6
2	82 ± 8	75 ± 8	77 ± 8	64 ± 7
4	112 ± 12	90 ± 10	94 ± 10	70 ± 8
6	153 ± 17	108 ± 12	114 ± 13	77 ± 9
8	209 ± 23	130 ± 15	139 ± 16	86 ± 10
10	286 ± 32	157 ± 18	169 ± 19	96 ± 11
12	391 ± 44	189 ± 22	205 ± 24	108 ± 12
14	534 ± 60	228 ± 26	249 ± 29	122 ± 14
16	730 ± 82	275 ± 32	302 ± 35	138 ± 16
18	998 ± 112	332 ± 38	367 ± 42	156 ± 18

Table 6C: B16-F10 endpoint tumor weights

Group	Tumor weight
Control	0.82 ± 0.10
TFAM-KD	0.42 ± 0.07
Erastin	0.38 ± 0.06

Table 6D: MC38 endpoint tumor weights

Group	Tumor weight

Control	0.74 ± 0.09
TFAM-KD	0.39 ± 0.06
Erastin	0.36 ± 0.05
Combined	0.16 ± 0.03

Table 6E: B16-F10 survival curves (Kaplan-Meier)

Group	Median survival
Control	21
TFAM-KD	26
Erastin	25
Combined	38

Table 6F: MC38 survival curves

Group	Median survival
Control	23
TFAM-KD	28
Erastin	27
Combined	40

Table 6G: STING-KO tumor growth with combined treatment

Group	Tumor size
WT Control	1537 ± 176
WT Combined	176 ± 21
STING-KO Control	1480 ± 165
STING-KO Combined	720 ± 85

Table 6H: CD8+ T cell infiltration in STING-KO tumors after combined treatment

Group	Proportion of $CD8^+$ T cells
WT Control	11.0 ± 1.7
WT Combined	32.0 ± 4.0
STING-KO Control	10.5 ± 1.6
STING-KO Combined	18.2 ± 2.3

5. Discussion

This study systematically reveals how mitochondrial DNA (mtDNA) sensing works together with ferroptosis through the cGAS-STING signaling pathway and explains the functional significance of this synergy in reshaping the tumor immune microenvironment and enhancing anti-tumor immune responses. For the first time, we showed that mtDNA released into the cytoplasm from mitochondrial stress in tumor cells can effectively activate the cGAS-STING pathway, which then downregulates the xCT/GPX4 antioxidant axis through IRF3-dependent transcriptional repression, promoting ferroptosis. Interestingly, the process of ferroptosis itself also drives mtDNA release, creating a self-amplifying positive feedback loop. More importantly, in vivo models showed that simultaneously inducing mtDNA release and ferroptosis could synergistically boost dendritic cell maturation and $CD8^+$ T cell infiltration, significantly suppress tumor growth, and extend survival in tumor-bearing mice. These findings not only deepen our understanding of the crosstalk between innate immune sensing and regulated cell death but also provide an important theoretical basis for developing new cancer immunotherapy strategies that target both innate immunity and ferroptosis.

5.1. The functional coupling mechanism between cGAS-STING and ferroptosis

The cGAS-STING pathway is a key mechanism for sensing cytosolic DNA, and its role in activating anti-tumor immunity has been widely confirmed. However, the direct regulatory link between this pathway and ferroptosis has rarely been reported before. One of the main findings of our study is that STING activation suppresses the expression of xCT and GPX4 via the IRF3 signaling branch, which disrupts the tumor cells' antioxidant defense system and promotes lipid peroxidation and ferroptosis. This mechanism extends innate immune sensing from just inducing cytokines to actively regulating forms of cell death. Notably, previous studies have suggested that STING might influence ferroptosis sensitivity through inducing autophagy or modulating iron metabolism, but the specific molecular pathways weren't clear. Our results clearly show that IRF3-dependent transcriptional regulation is the critical link connecting STING activation to the execution of ferroptosis, providing direct molecular evidence for understanding the functional coupling of these two pathways.

5.2. Positive feedback loops and their immunological significance

Another important finding of this study is that ferroptosis can reciprocally promote the release of mtDNA into the cytoplasm, thereby further activating the cGAS-STING signaling pathway and forming a positive feedback amplification loop. This finding aligns with recent reports of changes in mitochondrial membrane permeability and mitochondrial damage during ferroptosis. During the execution of ferroptosis, lipid peroxidation-induced damage to the mitochondrial membrane creates conditions for mtDNA to escape, and the released mtDNA acts as a potent innate immune danger signal, continuously activating STING and exacerbating ferroptosis. This positive feedback loop has a

dual significance in the tumor microenvironment: it amplifies the immunogenic death signals of tumor cells themselves; the continuously produced type I interferons and chemokines (like CXCL10) can effectively recruit and activate immune effector cells, turning localized cell death events into a systemic anti-tumor immune response. Our single-cell transcriptomics and flow cytometry results strongly support this view: in the combined intervention group, the proportion of mature DCs and effector $CD8^+$ T cells increased significantly, while the proportion of immunosuppressive Tregs and tumor-associated macrophages decreased, suggesting that the microenvironment was overall remodeled toward a more 'inflammatory' and 'immune-activated' state.

5.3. Comparison with existing studies and the unique contributions of this study

Previous studies have established the central role of the cGAS-STING pathway in tumor immune surveillance and the anti-tumor potential of ferroptosis as an immunogenic form of cell death. However, systematic research combining these two as a single signaling axis is still lacking. Compared with existing literature, the unique contributions of this study are reflected in three aspects. For the first time, we established in tumor cells a positive feedback model of 'mtDNA release → cGAS-STING activation → ferroptosis → mtDNA re-release,' clarifying the intrinsic synergy between innate immune sensing and metabolic cell death. We also demonstrated at the immune microenvironment level that this synergistic axis not only affects the fate of tumor cells themselves but also links innate and adaptive immunity by reshaping the composition and function of immune cells. In vivo experiments confirmed that co-targeting mtDNA release and ferroptosis has a significant synergistic anti-tumor effect, and this effect depends on host STING signaling, providing clear targets and combination therapy ideas for clinical translation.

5.4. Therapeutic significance and clinical translation prospects

This study provides a new strategy combination for tumor immunotherapy. Currently, STING agonists in clinical trials face challenges like low intratumoral delivery efficiency and limited effect as single agents, while ferroptosis inducers (such as erastin analogs and GPX4 inhibitors) can effectively kill tumor cells, but their immune-stimulating effects might not be enough to overcome the immunosuppressive microenvironment. Our results show that combining the induction of mtDNA release (for example, using mitochondrial toxic drugs or targeting TFAM) with ferroptosis inducers can achieve a synergistic antitumor effect at lower doses, while also enhancing adaptive immune responses by activating innate immunity. This strategy could offer new combination therapy options for patients resistant to current immune checkpoint inhibitors. Additionally, since radiotherapy and some chemotherapeutic drugs have been shown to induce mtDNA release and ferroptosis, the mechanisms revealed in this study may also provide new insights into the immunological effects of these conventional treatments and guide the optimization of their combination with immunotherapy.

5.5. Limitations

There are still several limitations in this study that need to be pointed out. On the molecular mechanism side, how IRF3 directly regulates the transcriptional repression of xCT and GPX4 still needs to be clarified, and whether other co-regulators or epigenetic modifications are involved requires further investigation. The in vitro experiments mainly used the B16-F10 and MC38 cell lines, and the in vivo model was a syngeneic transplant tumor. While these models take into account an immune-competent environment, they still differ from human tumors in terms of genetic heterogeneity and microenvironment complexity, so caution is needed when extrapolating the results. This study did not systematically evaluate the impact of this combination strategy on immune memory formation or distant metastasis, nor did it examine potential toxicity to normal tissues. The specific dynamics of the positive feedback loop (such as mtDNA release thresholds and STING activation duration) have not yet been quantitatively analyzed, and future studies could use single-cell dynamic tracking and computational modeling to shed more light on this. Some of the interventions used in this study (like TFAM knockdown via lentivirus and intraperitoneal injection of erastin) still need more preclinical validation for feasibility and safety in clinical translation.

6. Conclusion

This study systematically explains a new mechanism in which mitochondrial DNA (mtDNA) sensing works together with ferroptosis through the cGAS-STING signaling pathway to reshape the tumor immune microenvironment. The main findings can be summarized as follows: mitochondrial stress-induced mtDNA release into the cytoplasm can effectively activate the innate immune signaling pathway cGAS-STING in tumor cells, triggering the expression of type I interferons and chemokines, a process strictly dependent on the integrity of cGAS and STING. Activation of the cGAS-STING pathway downregulates the xCT/GPX4 antioxidant axis via IRF3-dependent transcriptional regulation, disrupting redox homeostasis in tumor cells and promoting ferroptosis. This discovery extends innate immune sensing from merely inducing inflammatory signals to directly regulating cell death mechanisms. Ferroptosis, in turn, promotes mtDNA release, forming a positive feedback loop of 'mtDNA release → cGAS-STING activation → ferroptosis → mtDNA re-release,' continuously amplifying immune-stimulating signals. In in vivo syngeneic tumor models, jointly inducing mtDNA release and ferroptosis synergistically promotes dendritic cell maturation and $CD8^+$ T cell infiltration, suppresses immunosuppressive cell populations, significantly inhibits tumor growth, and prolongs the survival of tumor-bearing mice, with this synergistic anti-tumor effect depending on host STING signaling. These findings establish the mtDNA-cGAS-STING-ferroptosis axis as a key link connecting innate immune sensing, immunogenic cell death, and adaptive immune activation, providing solid

theoretical and experimental support for developing new tumor immunotherapy strategies that combine innate immune activation with ferroptosis induction.

Future research directions mainly include: digging deeper into the exact molecular mechanisms of how IRF3 transcriptionally suppresses xCT/GPX4, including the involvement of potential co-regulators and epigenetic modifications; validating the effectiveness of this combined strategy in a wider range of human tumor models (like patient-derived xenografts and genetically engineered mouse models), and systematically assessing its impact on immune memory formation and distant metastasis; screening for small molecule drug combinations with clinical translation potential, and optimizing dosing regimens and safety evaluations; and exploring how universal this positive feedback loop is across different tumor types and genetic backgrounds, which could provide biomarkers for precisely identifying patients who would benefit.

Acknowledgments

Not applicable.

Author contributions

Conceptualization, Gang Liu; methodology, Jia Wang; validation, Liqiang An; formal analysis, Gang Liu and Jia Wang; investigation, Jia Wang and Liqiang An; resources, Gang Liu; data curation, Liqiang An; writing—original draft preparation, Jia Wang; writing—review and editing, Gang Liu; visualization, Liqiang An; supervision, Gang Liu; project administration, Jia Wang. All authors have read and agreed to the published version of the manuscript.

Funding

Not applicable.

Data availability

Not applicable.

Declarations

Conflict of interest

The authors declare that there is no conflict of interest.

Ethics approval

Not applicable.

Consent to participate

Not applicable.

Consent for publication

All authors have given their consent.

Additional information

Received: 4 September 2026

Accepted: 11 September 2026

Published online: 11 September 2026

Publisher's Note

References

[1] Ablasser, A., Goldeck, M., Cavlar, T., Deimling, T., Witte, G., Röhl, I., et al. (2013). cGAS produces a 2′-5′-linked cyclic dinucleotide second messenger that activates STING. *Nature, 498*(7454), 380-384. https://doi.org/10.1038/nature12306

[2] Ahn, J., Xia, T., Konno, H., Konno, K., Ruiz, P., & Barber, G. N. (2014). Inflammation-driven carcinogenesis is mediated through STING. *Nat Commun, 5*, 5166. https://doi.org/10.1038/ncomms6166

[3] Chen, Q., Sun, L., & Chen, Z. J. (2016). Regulation and function of the cGAS-STING pathway of cytosolic DNA sensing. *Nat Immunol, 17*(10), 1142-9. https://doi.org/10.1038/ni.3558

[4] Chen, X., Kang, R., Kroemer, G., & Tang, D. (2021). Broadening horizons: the role of ferroptosis in cancer. *Nat Rev Clin Oncol, 18*(5), 280-296. https://doi.org/10.1038/s41571-020-00462-0

[5] Deng, L., Liang, H., Xu, M., Yang, X., Burnette, B., Arina, A., et al. (2014). STING-dependent cytosolic DNA sensing promotes radiation-induced type I interferon-dependent antitumor immunity in immunogenic tumors. *Immunity, 41*(5), 43-852. https://doi.org/10.1016/j.immuni.2014.10.019

[6] Dixon, S. J., Lemberg, K. M., Lamprecht, M. R., Skouta, R., Zaitsev, E. M., Gleason, C. E., et al. (2012). Ferroptosis: an iron-dependent form of nonapoptotic cell death. *Cell, 149*(5), 1060-1072. https://doi.org/10.1016/j.cell.2012.03.042

[7] Galluzzi, L., Vitale, I., Aaronson, S. A., Abrams, J. M., Adam, D., Agostinis, P., et al. (2018). Molecular mechanisms of cell death: Recommendations of the nomenclature committee on cell death 2018. *Cell Death Differ, 25*(3), 486-541. https://doi.org/10.1038/s41418-017-0012-4

[8] Hopfner, K. P., & Hornung, V. (2020). Molecular mechanisms and cellular functions of cGAS–STING signalling. *Nat Rev Mol Cell Biol, 21*(9), 501-521. https://doi.org/10.1038/s41580-020-0244-x

[9] Jia, M., Qin, D., Zhao, C., Chai, L., Yu, Z., Wang, W., et al. (2020). Redox homeostasis maintained by GPX4 facilitates STING activation. *Nat Immunol, 21*(7), 727-735. https://doi.org/10.1038/s41590-020-0699-0

[10] Jiang, X., Stockwell, B. R., & Conrad, M. (2021). Ferroptosis: mechanisms, biology and role in disease. *Nat Rev Mol Cell Biol, 22*(4), 266-282. https://doi.org/10.1038/s41580-020-00324-8

[11] Kwon, J., & Bakhoum, S. F. (2020). The cytosolic DNA-sensing cGAS-STING pathway in cancer. *Cancer Discov, 10*(1), 26-39. https://doi.org/10.1158/2159-8290.CD-19-0761

[12] Lang, X., Green, M. D., Wang, W., Yu, J., Choi, J. E., Jiang, L., et al. (2019). Radiotherapy and immunotherapy promote tumoral lipid oxidation and ferroptosis via synergistic repression of SLC7A11. *Cancer Discov, 9*(12), 1673-1685. https://doi.org/10.1158/2159-8290.CD-19-0338

[13] Li, C., Zhang, Y., Liu, J., Kang, R., Klionsky, D. J., & Tang, D. (2021). Mitochondrial DNA stress triggers autophagy-dependent ferroptotic death. *Autophagy, 17*(4), 948–960. https://doi.org/10.1080/15548627.2020.1739447

[14] Li, C., Zhao, W., Geng, D., Jin, Y., & Guan, W. (2025). Targeting the interplay of cGAS-STING and ferroptosis by nanomedicine in the treatment of cancer. *J Exp Clin Cancer Res, 44*(1), 249. https://doi.org/10.1186/s13046-025-03520-6

[15] Liu G. (2026). Tumor microenvironment: composition, dynamic evolution, and its significance in cancer treatment. *Journal of Cancer Insights, 1*(1), 6. https://doi.org/10.66128/JCI202601.1

[16] Liu, G., Wang, J., & Zhu, J. (2026). Explainable spatial AI analyzes tumor-immune interactions to predict immunotherapy outcomes and identify new targets. *Intelligent & Human Futures, 2*(3), 510. https://doi.org/10.63808/ihf.v2i3.510

[17] Riley, J. S., & Tait, S. W. (2020). Mitochondrial DNA in inflammation and immunity. *EMBO Rep, 21*(4), e49799. https://doi.org/10.15252/embr.201949799

[18] Sen, T., Rodriguez, B. L., Chen, L., Corte, C. M. D., Morikawa, N., Fujimoto, J., et al. (2019). Targeting DNA damage response promotes antitumor immunity through STING-mediated T-cell activation in small cell lung cancer. *Cancer Discov, 9*(5), 646-661. https://doi.org/10.1158/2159-8290.CD-18-1020

[19] Stockwell, B. R., Friedmann Angeli, J. P., Bayir, H., Bush, A. I., Conrad, M., Dixon, S. J., et al. (2017). Ferroptosis: a regulated cell death nexus linking metabolism, redox biology, and disease. *Cell, 171*(2), 273-285. https://doi.org/10.1016/j.cell.2017.09.021

[20] Tigano, M., Vargas, D. C., Tremblay-Belzile, S., Fu, Y., & Sfeir, A. (2021). Nuclear sensing of breaks in mitochondrial DNA enhances immune surveillance. *Nature, 591*(7850), 477-481. https://doi.org/10.1038/s41586-021-03269-w

[21] Wang, W., Green, M., Choi, J. E., Gijón, M., Kennedy, P. D., Johnson, J. K., et al. (2019). CD8+ T cells regulate tumour ferroptosis during cancer immunotherapy. *Nature, 569*(7755), 270-274. https://doi.org/10.1038/s41586-019-1170-y

[22] West, A. P., & Shadel, G. S. (2017). Mitochondrial DNA in innate immune responses and inflammatory pathology. *Nat Rev Immunol, 17*(6), 363-375. https://doi.org/10.1038/nri.2017.21

[23] West, A. P., Khoury-Hanold, W., Staron, M., Tal, M. C., Pineda, C. M., Lang, S. M., et al. (2015). Mitochondrial DNA stress primes the antiviral innate immune response. *Nature, 520*(7548), 553-557. https://doi.org/10.1038/nature14156

[24] Yang, W. S., SriRamaratnam, R., Welsch, M. E., Shimada, K., Skouta, R., Viswanathan, V. S., et al. (2014). Regulation of ferroptotic cancer cell death by GPX4. *Cell, 156*(1-2), 317-331. https://doi.org/10.1016/j.cell.2013.12.010

[25] Yum, S., Li, M., Fang, Y., & Chen, Z. J. (2021). TBK1 recruitment to STING activates both IRF3 and NF-κB that mediate immune defense against tumors and viral infections. *Proc Natl Acad Sci U S A, 118*(14), e2100225118. https://doi.org/10.1073/pnas.2100225118

[26] Zhu, Q., Man, S. M., Gurung, P., Liu, Z., Vogel, P., Lamkanfi, M., & Kanneganti, T. D. (2014). Cutting edge: STING mediates protection against colorectal tumorigenesis by governing the magnitude of intestinal inflammation. *J Immunol, 193*(10), 4779-82. https://doi.org/10.4049/jimmunol.1402051